FOI-R--1650--SE
June 2005
ISSN 1650-1942
Technical Report

Magnus Berglund, Niklas Wikström, Christer Fureby

Numerical Simulation of Scramjet Combustion

Weapons and Protection
SE-147 25 TUMBA

THE SWEDISH DEFENCE RESEARCH AGENCY– FOI

Weapons and Protection
SE-147 25 Tumba

FOI-R--1650--SE

June 2005

ISSN 1650-1942

Technical Report

Magnus Berglund, Niklas Wikström, Christer Fureby

Numerical Simulation of Scramjet Combustion

Issuing organization	Report number, ISRN	Report type
FOI – Swedish Defence Research Agency Weapons and Protection SE-147 25 Tumba	FOI-R--1650--SE	Technical Report
	Research area code 5. Combat	
	Month year June 2005	**Project no.** E2006
	Customers code 5. Contracted Research	
	Sub area code 51. Weapons and Protection	

Author/s (editor/s)	Project manager
Magnus Berglund Niklas Wikström Christer Fureby	Bengt Eiderfors
	Approved by Torgny Carlsson
	Scientifically and technically responsible Christer Fureby

Report title

Numerical Simulation of Scramjet Combustion

Abstract (not more than 200 words)

In this study, Large Eddy Simulation (LES) has been used to examine supersonic flow and combustion in a model scramjet combustor. The LES model is based on an unstructured finite volume discretization, using total variational diminishing flux reconstruction, of the filtered continuity, momentum, enthalpy and mixture fraction equations. The configuration used is similar to the laboratory scramjet at the Institute for Chemical Propulsion of the German Aerospace Center (DLR) and consists of a one-sided divergent channel with a wedge-shaped flameholder at the base of which hydrogen is injected. Three cases are investigated: (i) supersonic flow, (ii) supersonic flow with hydrogen injection and (iii) supersonic flow with hydrogen injection and combustion. For the purpose of validation, the LES results are compared with experimental data for velocity and temperature at different cross-sections. In addition, qualitative comparisons are also made between predicted and measured schlieren, shadow and PIV fields. The LES computations are capable of predicting both the non-reacting and reacting flowfields reasonably well – in particular we notice that the LES model identifies and differentiates between peculiarities of the flow-fields found in the experiments.

Keywords

Scramjet combustion, large eddy simulation, experimental comparison

Further bibliographic information	Language English
ISSN 1650-1942	**Pages** 31
	Price acc. to pricelist **Security classification**

Utgivare	Rapportnummer, ISRN	Klassificering
Totalförsvarets Forskningsinstitut - FOI Vapen och skydd 147 25 Tumba	FOI-R--1650-SE	Teknisk rapport
	Forskningsområde 5. Bekämpning	
	Månad, år Juni 2005	**Projektnummer** E2006
	Verksamhetsgren 5. Uppdragsfinansierad verksamhet	
	Delområde 51 VVS med styrda vapen	

Författare/redaktör	Projektledare
Magnus Berglund Niklas Wikström Christer Fureby	Bengt Eiderfors
	Godkänd av Torgny Carlsson
	Tekniskt och/eller vetenskapligt ansvarig Christer Fureby

Rapportens titel

Numerisk simulering av scramjetförbränning

Sammanfattning (högst 200 ord)

I den här studien har storvirvelsimulering (LES, efter eng. Large Eddy Simulation) använts för att undersöka överljudsströmning och förbränning i en modell av en scramjetmotor. LES-modellen baseras på en ostrukturerad finita-volymsdiskretisering av kontinuitets-, rörelsemängds-, entalpi- och blandningsfraktionsekvationerna. Diskretiseringen använder en variationsminimerande fluxrekonstruktion av de konvektiva fluxerna för att undvika ofysikaliska oscillationer. Den konfiguration som används är en förenklad modell av en laboratoriemodell av en scramjetmotor vid Institutet for kemisk framdrivning vid det Tyska luft- och rymdfartsinstitutet (DLR) och består av en ensidig divergent kanal med en kilformad flamhållare vid vilkens bas vätgas injiceras i en överljudsströmning med luft. Tre fallstudier har genomförts: (i) enbart överljudsströmning, (ii) överljudsströmning med vätgasinjektion och (iii) överljudsströmning med vätgasinjektion och förbränning. I syfte att validera LES-modellen jämförs resultaten med experimentella data för hastighet och jämförelser görs även mellan förväntade och uppmätta schlieren-, skugg- och PIV fält. LES-beräkningarna har förmågan att förutse både ren strömning och kemiskt reagerande strömning förhållandevis väl.

Nyckelord

Scramjet förbränning, storvirvelsimulering, experimentella jämförelser

Övriga bibliografiska uppgifter	Språk Engelska
ISSN 1650-1942	**Antal sidor:** 31
Distribution enligt missiv	**Pris: Enligt prislista** **Sekretess**

List of Contents

Sammanfattning

Scramjet är en akronym för Supersonic Combustion Ramjet och är en motortyp som i likhet med ram- och jetmotorer utnyttjar reaktionsprincipen, men är utvecklad för högre flyghastigheter, eller Mach-tal. Vid Mach-tal större än fem låter man, till skillnad från rammotorn, förbränningen ske under överljudsförhållanden, vilket i sin tur ställer andra krav på inlopps-, utlopps- och brännkammargeometrierna. I likhet med ramjetmotorn har scramjetmotorn inte heller några rörliga delar vilket gör den mekaniskt enkel men aerodynamiskt betydligt mer komplicerad än t.ex. en jetmotor och den drivs ofta med vätgas. Eftersom hastigheterna i brännkammaren är så höga kommer uppehållstiden i brännkammaren att vara mycket kort, och under denna korta tid skall bränsle och luft blandas och reagera innan bränsleblandningen hunnit lämna brännkammaren. Strömningen i brännkammaren är således av central betydelse för att en effektiv förbränningsprocess skall kunna äga rum, och komplicerad då den innehåller samverkande stötar, skjuvskikt och virvelstrukturer. I vidstående rapport presenteras resultat från numeriska strömnings- och förbränningsberäkningar av en scramjetmotor. Den konfiguration som används är en laboratoriemodell av en scramjetmotor vid Institutet for kemisk framdrivning vid det Tyska luft- och rymdfartsinstitutet (DLR) och består av en ensidig divergent kanal med en kilformad flamhållare vid vilkens bas vätgas injiceras i en överljudsströmning med luft. Simuleringsmodellen har periodiska randvillkor i djupled och omfattar endast tre av femton jetstrålar hos den experimentella konfigurationen. Trots detta används 3.3 miljoner beräkningsceller. Beräkningsmodellen utnyttjar LES (storvirvelsimulering efter eng. Large Eddy Simulation) och baseras på en ostrukturerad finita-volymsdiskretisering av kontinuitets-, rörelsemängds- och energiekvationerna samt en variationsminimerande fluxrekonstruktion av de konvektiva fluxerna. Ekvationerna integreras i tiden med hjälp av en variationsminimerande Runge-Kutta metod av andra ordningens noggrannhet. I syfte att validera LES modellen görs kvalitativa och kvantitativa jämförelser med experimentella data för tre fall: (i) strömning genom brännkammaren utan vätgasinjektion och förbränning, (ii) strömning genom brännkammaren med vätgasinjektion men utan förbränning, och (iii) strömning genom brännkammaren med vätgasinjektion och förbränning. Kvalitativa jämförelser mellan beräkningar och experiment görs i ett område bakom flamhållaren där man i experimenten avbildat strömningen och flamman med hjälp av olika beröringsfria laserbaserade tekniker såsom slir-, skugg- och Rayleighavbildning. Kvantitativa jämförelser mellan beräkningar och experiment görs längs ett fåtal tvärsnittslinjer genom brännkammaren där man mätt hastighet och temperatur med hjälp av LDV och PIV (efter eng. Laser Doppler Velocimetry och Particle Image Velocimetry) tekniker. För enbart strömning och strömning med vätgasinjektion erhålls mycket bra överensstämmelse mellan experiment och beräkningar, medan vid strömning med vätgasinjektion och förbränning erhålls en något sämre överensstämmelse. Orsaken till detta är att den förbränningsmodell som använts är för enkel, då den inte kan ta full hänsyn till hur fort de kemiska reaktionerna fortskrider. Detta blir speciellt viktigt vid supersonisk förbränning då strömningens tidsskalor blir av samma storleksordning som omblandningens och förbränningens tidsskalor. En mer realistisk förbränningsmodell har utvecklats och testas just nu på föreliggande problem. Preliminära resultat indikerar att denna nya modell ger bättre kvalitativ och kvantitativ överensstämmelse med experimentella data, vilket kommer att redovisas separat.

1. Introduction

The current road map of aerospace technology development contains several areas of application for hypersonic vehicles such as cruise missiles (which would represent a radical breakthrough for the present military doctrines), long range passenger transport and reusable launch vehicle for space applications. For example, an advanced Mach 5 passenger aircraft would be capable of decreasing the flight time from Europe to the United States (a distance of about 7,500 km) to 1.5 hours and from Europe to Australia to 3 hours – a factor of 5 in comparison with current values. Reusable launch vehicle for space applications (either in Single Stage To Orbit (SSTO) or Two Stage To Orbit (TSTO) configurations) will have the possibility of lowering the price of launching payloads to the low earth orbit from current value of about 75 kSEK/kg down to about 7.5 kSEK/kg, which is considered a necessary prerequisite for the successful commercial utilization of space and for a possible future exploration of the solar system.

The successful development of such flying vehicles would depend, to a large extent, on the development of an efficient propulsion system. Turbojets, which are the most commonly used propulsion systems for subsonic and moderately supersonic aircrafts, cannot be operated beyond Ma≈3 due to the high temperature and pressure (about 650 K and 0.43 bar) in front of the air intake, i.e. before the compressor, from a materials point of view. Rocket engines, presently used in space launcher systems, are unattractive (at least for endo-atmospheric vehicles) due to their poor fuel economy and their low safety. The propulsion system of choice for flight in the supersonic (Ma=3-5) regime is a ramjet and beyond that in the hypersonic (Ma=5-15) regime is a ramjet with supersonic combustion, i.e. a scramjet. When a ramjet flies at supersonic speed, the internal airflow remains subsonic because it has to be slowed down to reach the high temperatures and pressures required. At higher speeds (Ma=6-7), the slowdown of the internal airflow causes a dramatic increase of the losses: the air is too hot and the engine no longer works efficiently. The best solution is to slow down the airflow, but not below supersonic speeds, at which a ramjet with a supersonic combustion process, i.e. a scramjet, results. If the internal flow is supersonic, the air is not slowed down as much, it is colder, and the fuel stays only a very short time (about 1 ms) in the combustion chamber. During this short period of time, the fuel has to be mixed on a molecular level with the air and the reactions have to be completed before leaving the engine. Scramjet combustion experiments are extremely complicated, and only a few limited run-time facilities are available. The most cost-efficient way of investigating the propulsion system performance at these flight regimes, therefore, lies in the use of sophisticated computer simulations, provided that the simulation models have the required accuracy. Over the last quarter of century, Computational Fluid Dynamics (CFD) has gradually become a major research tool, playing an extensive role in aerospace science development. In addition to allowing the analysis of flow conditions which can not be readily obtained otherwise, CFD can reduce the length and cost of the design cycle, due to the continuous advances in computer technology and the development of more sophisticated models and flow simulation codes.

In this report we will, besides giving a brief historical overview of the scramjet engine development, present some of the technological challenges facing the development of scramjet engines that can be investigated by CFD. Moreover, we will discuss the development of accurate and robust CFD models for supersonic combustion, and show examples of their use in predicting hypersonic flows as well as scramjet combustion. These computational examples are chosen so that the computations can be compared to detailed experiments, providing validation of the CFD model. When successfully validated the CFD model can be used to gain further understanding of

the experiments since much more information is generally available from the simulation model than from the experiments. Next, the simulation model can be used to further explore other flow and combustion regimes as well as other novel engine designs.

In Section 2 some historical notes on scramjet engine development will be provided to facilitate a proper background for Section 3, which deals with selected technical challenges for scramjet engines. Section 4 addresses the issues of mathematical and numerical modeling of scramjet combustion and is of more technical nature than the remaining report. In section 5 we describe the DLR scramjet experimental rig that will be used as a representative validation test case. In Section 6 the results of the simulations of flow, mixing and combustion are presented and compared with the available experimental data. Finally, in Section 7 we provide an outlook focusing on how accurate and useful high-fidelity CFD simulations will be for the future development of scramjet engines, and some concluding remarks.

2. Historical Notes on Scramjet Engine Development

Supersonic combustion air-breathing engines have long been recognized as the most well-suited for hypersonic propulsion in the Ma 5 to 15 range. Designs for hypersonic engines have been around since the early 1900's. The first theoretical studies and patents of the ramjet principle were realized in the 1920's. At the 1938 Paris air-show, an aircraft with an integrated ramjet engine for subsonic flight velocities, designed by R. Leduc, was presented. During and after World War II, tremendous effort was put into research on high-speed jet- and rocket-powered aircraft. Supersonic air-intakes was developed in Germany and some practical devices were realized, notably gun-launched supersonic ramjets (later introduced in the Soviet Armed Forces) and ramjets for solid fuels and even ramjets for driving helicopter rotors. After the war, Leduc continued work with his concept and realized flights with a Ma number of about 0.9. The French company Nord-Aviation continued this approach and realized an aircraft powered by a hybrid turbo-ramjet engine. The turbojet was used at take-off and the ramjet could be gradually activated as the flight speed increased. Ma numbers around 2 were achieved at 18 km altitude, and the primary application was surface-to-air missiles. This doctrine and the corresponding realization was followed by England, France and the Soviet Union. Typically, the missile was accelerated from ground by a solid-propellant rocket-booster after which the ramjet ignited. The range varied between 50 and 100 km at an altitude of about 30 km at Ma numbers between 2 and 3. In the US, the Bell X-1 attained supersonic flight in 1947, and by the early 1960's, rapid progress towards faster vehicles suggested that operational aircraft would be flying at hypersonic speeds within a few years. Except for specialized rocket research vehicles like the US X-15 and other rocket-powered spacecraft, aircraft top speeds have remained at Ma ≈2.

Figure 1. X-15 high-speed research plane shortly after launch. Photo taken from www.aerospaceweb.org.

In recent years, significant progress has been made in the development of hypersonic technology, particularly in the field of scramjet engines. The US Army desires hypersonic missiles that can attack mobile missile launchers quickly. NASA believes hypersonics could help develop economical, reusable launch vehicles. The US Air Force is interested in a wide range of hyper-

sonic systems, from air-launched cruise missiles to orbital spaceplanes to regain the international initiative. While US efforts are the best funded, the first to demonstrate a scramjet working in an atmospheric test was the Australian HyShot project at the University of Queensland that principally demonstrated scramjet combustion in 2002. The HyShot team took a unique approach to the problem of accelerating the engine to the necessary speed by using an Orion-Terrier rocket to attain a parabolic trajectory to an altitude of 314 km. As the craft re-entered the atmosphere, it dropped to a speed of Ma 7.6. The scramjet engine then started, and it flew at Ma 7.6 for about 6 s. Another very early scramjet demonstration was made on November 17, 1992, when Russian and French scientists successfully launched a scramjet engine in Kazakhstan. From 1994 to 1998 NASA worked with the Russian central institute of aviation motors (CIAM) to test a dual-mode scramjet engine. Four tests took place at Ma≈5.5, 5.3, 5.8 and 6.5, respectively. The final test took place aboard a modified SA-5 surface to air missile launched at the Sary-Shagan test range in the Republic of Kazakhstan on 12 February 1998. Data regarding whether the internal combustion took place in supersonic air streams was inconclusive.

The most advanced US hypersonics program is the NASA Langley Hyper-X program that is the successor to the National Aerospace Plane (NASP) program that was cancelled late 1994. This program involves flight-testing through the construction of the X-43 vehicles. The first, the X-43A is a 3.6 m long scramjet-powered research vehicle constructed by MicroCraft Inc. (now Alliant Techsystems Inc.). Three X-43A aircraft were developed for NASA, to be flown aboard modified Pegasus rockets. The Pegasus is dropped by a B-52 aircraft and launched to an altitude of over 27,500 m, where the X-43A is released and flown under its own power. Each of the three vehicles appears identical but have slightly different air intake designs, based on what speed their test flights are planned to accomplish. The first successful flight was undertaken on March 27, 2004, following the disastrous first attempt of June 2, 2001. The first flight set a new speed record of Ma 7, its engine running for 11 s, whereas the third flight on November 16, 2004, approached Ma 9. Three follow-on projects are discussed: The X-43B, which is a scaled-up version of the X-43A to be powered by the ISTAR engine. ISTAR will use a hydrocarbon-based liquid-rocket mode for initial boost, a ramjet mode for speeds above Ma 2.5, and a scramjet mode for speeds above Ma 5 to take it to maximum speeds of at least Ma 7. X-43C is a version of X-43A that would use the HyTECH hydrocarbon-fueled scramjet engine. Whilst most scramjet designs to date have used hydrogen as fuel, HyTECH runs on conventional kerosene fuels which are more practical for support of operational vehicles. A full-scale engine is being built, which will use its own fuel for cooling. Using fuel for engine cooling is nothing new, however, the cooling system will act as a chemical reactor, breaking long-chain hydrocarbons down to short-chain hydrocarbons that burn faster. Finally, X-43D is the most recently planned version of the X-43 craft, but with a hydrogen-powered scramjet engine with a desired maximum speed of about Ma 15.

Figure 2. NASA's X-43A undergoing ground testing. Photo taken from www.nasa.gov/missions/research.

Hypersonic development efforts are also in progress in other nations. Although the Australians were the first to unambiguously demonstrate a scramjet working in an atmospheric test suc-

cessful scramjet firings have also been performed in Russia, France and the USA. In addition, it is believed that also Japan and India have hypersonic programs aiming at developing or participating in developing scramjet test vehicles. The French are considering their own scramjet test vehicle and are in discussions with the Russians for boosters that would carry it to launch speeds. The approach is very similar to that used with the current NASA X-43 crafts. The notional immediate goal of the study is to produce a hypersonic air-to-surface missile, Promethee, which would be about 6 m long and weigh 1,700 kg. The Japanese scramjet effort is motivated by the slow-paced race to build the world's first true space plane – a civilian spaceliner. The research is mainly conducted at the Kakuda Propulsion Research Laboratory, but also involves Austrailan researchers from the University of Queensland. To avoid carrying liquid oxygen, a spaceplane would have to glean oxygen from the atmosphere and mix it with fuel, most likely liquid hydrogen, and burn the mixture inside a combustor to generate thrust. A plane like the SR-71, which has a ramjet mode (i.e. air is compressed by the internal shape of an engine), might be traveling at several times the speed of sound, but the air flowing into its engine has to be slowed to subsonic speeds to sustain combustion. A spaceplane would have to go so fast that sooner or later the air could no longer be slowed down sufficiently. Ramjet operation would be impossible after Ma 6, and the engine would have to operate as a supersonic ramjet or a scramjet.

Figure 3. The Japanese scramjet engine wind tunnel model. Photo taken from //www.aiaa.org/aerospace/Article.cfm

Figure 4. Test firings of the scramjet engine in Japan at Ma 8 flight conditions. Photo taken from //www.aiaa.org/aerospace/Article.cfm

3. Technical Challenges for Scramjet Engines

The basic elements of ram- and scramjet engines are an inlet that compresses the free-stream air from a hypersonic Ma number to roughly one-third that value, a combustor within which air mixes with fuel before reaction occurs, and an exhaust nozzle that expands the hot combustion products back to free-stream pressure. The fuel is often gaseous hydrogen, and because of the length scales, flow rates and pressures of applied interest, the mixing of fuel and air, and the combustion of the resulting mixtures involves turbulent flow. Dissociation caused by the large temperature increase of decelerating the flow from supersonic to subsonic speeds was a major drawback of the ramjet, Weber & MacKay, [1]. To minimize these effects, attention was focused on performing the combustion at supersonic speeds, in a scramjet, shown schematically in figure 5. In the scramjet, the inlet acts as a compressor. As the air approaches the engine, it passes through a system of shock waves produced by the inlet cone and edges of the air intake, reducing its velocity. The air velocity passing through the inlet is reduced slightly (but is still supersonic), while the static pressure increases by one or two orders of magnitude. At this point, the air enters

the combustion chamber and fuel is added. Fuel injection ports can either be mounted on the wall of the combustor chamber or on struts, allowing the fuel to be injected closer to the centerline of the chamber. The fuel-air mixture is then ignited and burned in a supersonic environment. This combustion process accelerates the flow to a speed slightly above the flight speed of the vehicle. After passing through the combustor, the gases enter the exit nozzle and are accelerated out the back of the engine. The thrust of a scramjet is produced by the change in momentum of the gases and pressure differences between the inlet and exit regions. Several variations and improvements have been implemented over the years to enhance this general scramjet cycle.

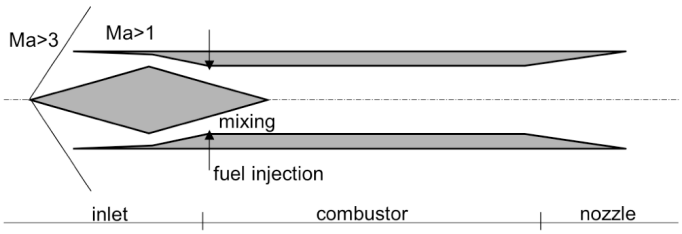

Figure 5. Schematic diagram of a generic scramjet engine showing the different engine parts and where fuel is injected into the supersonic flow.

3.1. Obstacles Encountered with Scramjet Combustion

Although the concept of scramjet engines appears simple, supersonic combustion is a complex field. Chemical kinetics, temperature, pressure, equivalence ratio, mixing rate and velocity all affect the combustion process. As it stands, supersonic combustion is very difficult to maintain and this continues to be a formidable task. The ignition delay time of a fuel-air mixture continues to be the limiting factor for all scramjet engine designs. Decreasing the delay time allows for shorter combustors and/or higher flight velocities. Initially, the ignition delay time of a fuel is fixed for a given set of conditions and the type of fuel. Increasing the temperature of the fuel and/or air stream reduces this time. Pressure plays a somewhat more complex role. Increasing the pressure, usually, but not always, improves the combustion conditions. Increasing pressure usually reduces the ignition delay time, but there exists a critical value of pressure, above which, the delay time increases dramatically, followed by a slow decrease. Therefore, it is not always advantageous to increase the pressure. The equivalence ratio does not strongly affect the ignition delay time, except for equivalence ratios below 0.3, where the delay time increases sharply. Therefore, these effects need to be considered in designs. Perhaps the largest problem associated with combustion is that of mixing. If fuel cannot be properly injected and mixed into the air stream it will not ignite, regardless of the pressure, temperature or equivalence ratio. Due to compressibility effects, fuel injection presents challenging obstacles. The air stream is at such a high pressure and velocity, that fuel injected into the stream has a tendency to be pushed against the wall and rendered ineffective. Another problem of concern is the aerodynamic heating of the confinement walls of the combustor that may require exotic materials and specific arrangements for cooling of the confinement walls. Also, at very high temperatures the reactants may start to dissociate prior to combustion, resulting in lower levels of heat release than expected at standard temperature and pressure. For example, at temperatures below about 1800 K the global reaction mechanism of hydrogen/oxygen combustion is,

$$H_2 + \tfrac{1}{2}O_2 \rightarrow H_2O, \quad \Delta h = -242\text{kJ}, \tag{1}$$

whereas at 5000 K the same global reaction mechanism becomes,

$$H_2 + \tfrac{1}{2}O_2 \rightarrow 0.86H_2 + 0.43O_2 + 0.14H_2O, \quad \Delta h = -34\text{kJ}, \tag{2}$$

suggesting that only a fraction of the chemical energy can be utilized. In addition to the problems of fuel-air mixing, high temperature combustion, and high thermal heat loads, ignition at these high velocities is extremely difficult. To overcome these challenges, several solutions have been proposed, and hereafter we will briefly review some of them.

3.2. Proposed Solutions to Supersonic Combustion Difficulties

Improved schemes for injection patterns have been designed and studied to overcome the obstacles of inadequate fuel penetration and mixing (Huber *et al.*, [2], Baurle *et al.*, [3], Schetz *et al.*, [4] and King, [5]). In addition, the problem of ignition and flame-holding can be handled in one of two ways; injecting combustion enhancing radicals by use of a plasma torch can reduce the induction time of the mixture (Sato *et al.*, [6], Kato *et al.*, [7], Wagner *et al.*, [8], Barbi *et al.*, [9] and Kimura *et al.*, [10]), or recirculation zones can be created using aerodynamic bodies such as wedges, ramps or cavities to slow down the flow and provide an environment where combustion can occur (Fujimori *et al.,* [11], Davis & Bowersox, [12], Yu *et al.*, [13], Baurle & Gruber, [14] and Sands *et al.*, [15]). Combinations of these methods can also be used.

Fuel Injection. Advanced fuel injector designs hold promise for solving mixing concerns. Numerous geometries have been tested to improve the mixing characteristics of fuel injection ports. These include swept ramps (Hartfield *et al.*, [16] and Donohue *et al.*, [17]), multiple ports (Cox *et al.,* [18] and Fuller *et al.*, [19]), inclined injection (McCann & Bowersox, [20]) and circular and non-circular geometries (Gruber *et al.*, [21]). One interesting concept using fuel injection is that of initiating detonation by interacting supersonic jets. Achasov *et al.* [22], discovered that a jet recessed into a small cavity with incident jets focused towards the center of the cavity could produce a region of high energy density which can lead to the onset of detonation. These jets enhanced the pressure and temperature within the volume of the cavity and produced a region of fast turbulent mixing. Another design implementing the use of jet interaction is one proposed by Schetz *et al.* [4], in which an aerodynamic ramp, rather than a physical one, is produced by means of nine differently-angled fuel ports. These ports were arranged to produce fuel-vortex interactions to enhance mixing in a supersonic cross-flow. Experiments conducted with this aero-ramp showed that with increased jet momentum, penetration increased, while a comparable physical ramp showed no significant improvement. Also noteworthy was that the total pressure losses induced by the aero-ramp were less than those of the physical ramp. Another method of fuel injection is to position the injectors on a strut. Huber *et al.*, [2], reported that auto-ignition of hydrogen occurred easier when injected from a strut than from a wall because of the smaller boundary layer and higher surface temperature of the strut. Masuya *et al.*, [23], later confirmed these findings, testing different strut designs in a Ma 2.5 airstream. In some cases, struts are superior to other aerodynamic shapes, such as wedges and cavities, because they do not significantly disturb the flow and have fewer losses associated with them. The shape of the jet is also important. Gruber *et al.*, [21] discovered that elliptical jets could enhance the mixing rate of fuel into a supersonic airstream. Elliptical jets tested in a Ma 2 cross-flow demonstrated increased spanwise spreading of the shear layer and greater turbulence intensity when compared to a circular jet. Shadowgraphs revealed that structures of the elliptical jet produces a smaller separation

region upstream of the jet and also produced a weaker bow shock. However, the elliptical jet also had reduced lateral penetration compared to the circular jet.

Recessed Cavity Flame-holders. Another promising method of mixing and flame-holding in supersonic environments comes from the use of recessed cavities. Experiments conducted by Yu *et al.*, [13], were designed to determine how the shape and interaction between multiple cavities affected the mixing capabilities of the flow. Normalized flame intensity images suggested that short cavities provided steady flame-holding. Longer cavities resulted in more compact, but intense flame structures. Finally, cavities with inclined downstream walls had very poor flame-holding capabilities. In general, cavities with small aspect ratios and vertical downstream walls appeared to be good flame-holders. In addition, Baurle & Gruber, [14], determined how the dimensions of the cavity affect the mixing characteristics. They found that the length of the cavity determined its mass entrainment capabilities, while the depth of the cavity determined the residence time. They also found that longer cavities had higher drag coefficients.

Ramps and Wedges. Ramps and wedges have long been used as bluff body flame-holders. The shock waves produced by their edges, and the rapid change of duct area just past the bluff-body enhance mixing. Typically, a fuel injector is located just downstream of the bluff body to take full advantage of the turbulence produced. Shock-induced combustion behind a wedge and ramp has been studied extensively. Shock waves are unavoidable in a scramjet combustor, but are not always detrimental. These shock waves can change the temperature, velocity and flame characteristics, affecting the combustion process. Fujimori *et al.*, [11], found that the recirculation behind a wedge in a supersonic air-stream was very sensitive to the fuel flow-rate. With low fuel flow-rates, most of the reaction occurred within the recirculation zone, but with higher flow-rates, the reaction zone moved away from the wedge and extinguished. Sands *et al.*, [15], proved analytically and experimentally that flame-holding was possible with a rectangular ramp. Although they have been proven adequate flame-holders, bluff-bodies also incure large flow losses due to low back-pressure as their cross-sectional area increases.

Plasma Torches. Plasma torches (or plasma igniters) have a wide range of application in industry and also come in many different forms. However, plasma torches of interest to scramjet engines are those that are used for ignition and flame-holding, e.g. Sato *et al.*, [6], Kato *et al.*, [7] and Kimura *et al.*, [10], and have proven useful at Ma numbers of about 6, Sato *et al.*, [6]. Regardless of the design, the purpose of a plasma torch is to ionize and dissociate the feedstock gas into hot, reactive plasma. In particular to produce combustion-enhancing radicals such as hydrogen, nitrogen and oxygen atoms, OH, C_2, OH and CH_3. Typically, the power range of these devices is limited to a few kilowatts to consume only the smallest possible fraction of the total engine power. The feedstock is generally hydrogen, nitrogen or a mixture of these, combined with argon. As the feedstock gas passes through an electric arc it is ionized, and in the case of more complex gases, also dissociated. This process produces combustion-enhancing radicals that reduce the reaction time for the combustion processes. This plasma is then injected into the fuel-air stream where the combustion reactions take place. Unlike a common candle or diffusion flame, plasma torches with choked constrictors are extremely difficult to blow out. For this reason they are well suited for supersonic combustion applications.

4. Mathematical and Numerical Modeling of Scramjet Combustion

When investigating scramjet combustion, and many other types of technical applications, two approaches, both guided by theory, are available: experiments and computations. The theoretical model generally consists of a system of non-linear partial differential equations that cannot be solved analytically, but numerical techniques must be invoked, resulting in the computational route. The experimental route is by far the oldest whereas the computational route has evolved in pace with the recent and rapid development of computers. In the experimental approach, test rigs are built at various scales: from full-scale engines to laboratory engines in model scale, in order to test or measure different aspects of the engine performance. The measurement techniques have however evolved dramatically during the last decades; from gas analysis probes, pressure probes and simple thermocouples inserted into the inlet, combustion chamber or nozzle, to non-intrusive laser-based methods that can be used to map entire regions of the flow and flame. This development in measurement techniques makes it possible to conduct realistic and very accurate engine tests in which several quantities such as temperature, species concentrations and velocity are measured simultaneously without affecting the operational behavior of the engine. The drawback is that these experiments are very difficult to set up and operate, and they are therefore extremely expensive. On the other hand, the rapid development of computers, and computational software, has enabled high-fidelity simulations of very complicated phenomena at reasonable cost. In these simulations the governing equations as well as space and time are discretized in a form usable by the computer. During the 80's the most advanced computers were the CRAY vector-machines, capable of performing 4 Gflops[1,2], during the 90's they were replaced by SGI, IBM and HP parallel supercomputers capable of performing ~10 Gflops[3], and during the 2000's they are in turn replaced by parallel linux clusters capable of performing >200 Gflops[4]. At the same time as the computational performance has increased from a few Gflops to a few Tflops the computational cost has decreased from 5 SEK/cpuh to 0.5 SEK/cpuh. Altogether, this means that we can now perform computational simulations of for example engine flows based on first principles at a reasonable cost. In turn, this puts new demands for more sophisticated and detailed measurements, leading to fewer experiments but conducted more carefully and with additional measurement equipment to gather more extensive information. These detailed experiments are used for two main purposes: to gain information of the engine operational performance, and to provide a validation database that can be used for developing improved simulation models.

Due to the complexity of scramjet combustion and the large computational resources required for undertaking such computations not much has been achieved. The most noteworthy computational studies so far have been carried out for the scramjet engine selected for this study. In 2000, Oevermann, [24], presented results from two-dimensional steady-state Reynolds Averaged Navier Stokes (RANS) calculations using an adaptive mesh together with a flamelet combustion model. In 2003 Genin *et al*, [25], presented results for the same case using Large Eddy Simulations (LES), using two different combustion models in a domain encompassing three jets and periodic boundary conditions in the spanwise direction. For both cases, reasonable results were obtained, but the LES results are in better qualitative agreement with the measurement data, since they are more realistic in mimicking the unsteady turbulent flow.

---

[1] flop = floating point operation per second.
[2] Cray2 at Lawrence Livermore National Laboratory (LLNL), CA, USA, 1985-89
[3] IBM ASCII Red at Sandia National Laboratory (SNL), NM, USA, 1995-2000
[4] IBM Blue Gene at Lawrence Livermore National Laboratory (LLNL), CA, USA, 2005-…

4.1. Theoretical Models for Chemically Reactive Flows

Irrespectively of whether we consider experiments or computations we need a theoretical model describing, mathematically, the processes that we are dealing with. For scramjet combustion, this mathematical model consists of the well-known conservation and balance equations of mass, momentum and energy, [26], for a given chemical reaction mechanism,

$$\begin{cases} \partial_t(\rho)+\nabla\cdot(\rho\mathbf{v})=0, \\ \partial_t(\rho Y_i)+\nabla\cdot(\rho\mathbf{v}Y_i)=\nabla\cdot\mathbf{j}_i+\dot{w}_i, \\ \partial_t(\rho\mathbf{v})+\nabla\cdot(\rho\mathbf{v}\otimes\mathbf{v})=-\nabla p+\nabla\cdot\mathbf{S}+\rho\mathbf{f}, \\ \partial_t(\rho E)+\nabla\cdot(\rho\mathbf{v}E)=\nabla\cdot((-p\mathbf{I}+\mathbf{S})\mathbf{v})+\nabla\cdot\mathbf{h}+\rho\sigma, \end{cases} \quad i=1,\ldots,N, \tag{3}$$

where ρ denotes the (mass) density, $\mathbf{v}$ the velocity, p the pressure, $\mathbf{S}$ the viscous stress tensor, $\mathbf{f}$ the body force, $E=e+\frac{1}{2}\mathbf{v}^2=h-p/\rho+\frac{1}{2}\mathbf{v}^2$ the total energy, where $e=h-p/\rho$ is the internal energy and h the enthalpy, $\mathbf{h}$ the heat flux vector, σ the non-mechanical energy supply (representing e.g. thermal radiation), Y_i the species mass-fraction, $\dot{w}_i$ the species reaction-rate and $\mathbf{j}_i$ the species mass-flux. In order to close (3) additional relations describing the fluid properties and the rate at which species i is produced or destroyed are needed. Again, following [26],

$$\begin{cases} \mathbf{j}_i=D_i\nabla Y_i, \\ \dot{w}_i=\sum_{j=1}^{M}(P''_{ij}-P'_{ij})\dot{w}_{ij}=\sum_{j=1}^{M}(P''_{ij}-P'_{ij})\left[k_{fj}\rho^{\sum_i P'_{ij}}\prod_{i=1}^{N}Y_i^{P'_{ij}}-k_{bj}\rho^{\sum_i P'_{ij}}\prod_{i=1}^{N}Y_i^{P''_{ij}}\right], \quad i=1,\ldots,N,\ j=1,\ldots,M, \\ p=\rho RT\sum_i(Y_i/M_i), \\ \mathbf{S}=(\lambda+\frac{2}{3}\mu)(\mathrm{tr}\mathbf{D})\mathbf{I}+2\mu\mathbf{D}_D, \\ h=\sum_i(Y_i h^{\theta}_{f,i})+\sum_i(Y_i\int_{T_0}^{T}C_{P,i}(T)dT), \\ \mathbf{h}=\kappa\nabla T, \end{cases} \tag{4}$$

where $\mathbf{D}=\frac{1}{2}(\nabla\mathbf{v}+\nabla\mathbf{v}^T)$ is the rate-of-strain tensor, $C_{P,i}$ the species heat-capacities, $h^{\theta}_{f,i}$ the species formation enthalpies, λ and μ the viscosities of the mixture, κ the heat conductivity of the mixture and D_i is the diffusivity of species i. Furthermore, k_{fj} and k_{bj} are the forward and backward rate constants, usually expressed in Arrhenius form $k_{fj}=A_j\exp(-T_{Aj}/T)$, where A_j and T_{Aj} are the pre-exponential factor and the activation temperature of the j^{th} reaction step.

The reacting Navier-Stokes Equations (NSE) (3)-(4) do not only represent convective, diffusive and local processes (i.e. chemistry) but also wavelike and oscillatory processes associated with shock and sound waves, as well as other transient processes, such as combustion-induced instabilities, cycle-to-cycle variations and combustion oscillations associated with unsteady vortex dynamics. Considering the involved processes, and their mutual interactions, it is evident that reacting flows are complicated, and constitute a formidable challenge to CFD. The most striking issue is the wide range of spatial and temporal scales that are represented in this mathematical model; the largest flow scales are the integral scales (v', ℓ and $\tau_I=\ell/v'$), and the smallest flow scales are the Kolmogorov scales ($\upsilon=(\nu\varepsilon)^{1/4}$, $\eta=(\nu^3/\varepsilon)^{1/4}$, and $\tau_K=(\nu/\varepsilon)^{1/2}$, where ε is the dissipation). Similarly, the characteristic chemical scales are the unstretched laminar flame speed S_u^0, the laminar flame thickness $\delta_u^0=\nu/S_u^0$, and the chemical reaction time $\tau_C=\delta_L^0/S_u^0$. A further complication arise in compressible flows where shocks and discontinuities are transformed into sharp but continuous variations due to viscosity and heat conduction. Hence, an internal structure over the shock-thickness, λ, arise, conditioned by a balance between viscous and thermal effects. For

scramjet flows η, δ_u^0 and λ are usually very small in comparison to the engine dimensions, and to resolve the processes that occur on these scales on the computational mesh, the mesh spacing, Δ, must be smaller than all of these quantities. In general, this will require such fine meshes that the number of mesh points will exceed the limit of what current computers can handle. The alternative is to model the effects of the small-scale physio-chemical processes, thereby reducing the mesh and the computational effort as will be elaborated on in Section 4.3.

4.2. Outstanding Issues for Scramjet Combustion

In high speed reactive flows, density variations arise from the heat release due to combustion and from both viscous heating and local compressions and expansions associated with the high velocities. The quantity which distinguishes these flows from the constant density turbulence treated extensively for centuries is the dilatation $\nabla\cdot\mathbf{v}$, which from conservation of mass can be seen to be directly related to the change in density. In low speed turbulent combustion the influence of pressure and velocity on the dilatation can virtually be neglected, and under these circumstances the dilatation is due only to the heat release. However, in high-speed combustion all of these influences play a role. Density variations due to heat release exist in both high and low speed combustion, whilst those due to compressibility arise only in high-speed flows. However, it is worth noting that as the speed of the flow increases the kinetic energy per unit mass, $\frac{1}{2}\mathbf{v}^2$, dominates the enthalpy per unit mass so that the heat release due to combustion adds relatively smaller amounts of energy as the Ma number increases. Accordingly, the influence of combustion on the flow becomes become less important as the Ma number increases.

Although there is some interest in high-speed turbulent combustion with hydrocarbon fuels, e.g. in the low Ma number regime, hydrogen is the fuel of choice for most applications. It is therefore of interest to consider the chemical kinetic behavior of the hydrogen-air system. A detailed description of the reaction steps involved is given in [27] and typically involves 18 reaction steps and the 9 species H_2, O_2, H_2O, O, H, OH, HO_2 and H_2O_2. If pollutants are also of concern this mechanism has to be extended to also include the nitrogen chemistry, resulting in e.g. NO and NO_2, e.g. Gutheil *et al*, [28]. Given the difficulties of including complex chemistry (e.g. short time scales and thin fronts) it is important to have available simplified chemical reaction mechanisms. One such example is the two-step mechanism of Rogers & Chinitz, [29], involving the four species H_2, O_2, H_2O and OH which can be expressed as,

$$\begin{cases} H_2 + O_2 \Leftrightarrow 2OH, \\ 2OH + H_2 \Leftrightarrow 2H_2O, \end{cases} \tag{5}$$

where $k_{fi} = A_i(\phi)T^{n_i}\exp(E_i/RT)$ is the Arrhenius reaction rate, and ϕ the equivalence ratio. The values of the coefficients A_i, n_i and E_i in this equation are presented in Table 1. Two-step mechanisms usually offer substantial improvement over the one-step mechanism (i.e. $H_2 + \frac{1}{2}O_2 \Leftrightarrow H_2O$)

Table 1. Reaction rate parameters for simplified two step hydrogen-air combustion with A_i in $m^3/(mol\cdot s\cdot K^{ni})$ and E_i in J/mol.

Reaction step 1	$A_1(\phi)=(8.917\phi+31.433/\phi-28.950)\cdot 10^{41}$ $E_1=20{,}384$ $n_1=-10$
Reaction step 2	$A_2(\phi)=(0.833\phi+1.333/\phi+2.0)\cdot 10^{58}$ $E_2=178{,}000$ $n_2=-13$

and simply by allowing the radical recombination reaction to be reversible could possibly provide a reasonable description of high temperature ignition when the flamelets experience rate-of-strain effects. However, at sufficiently high temperatures more detailed mechanism have to be included to cover the aforementioned dissociation effects. Other useful two-step mechanisms are proposed by Trevino & Mauss, [30], and Balakrishnan *et al.*, [31].

Low speed combustion is commonly characterized by the length and time scales (v', ℓ, τ_I, etc.) introduced in Section 4.1. To characterize high speed combustion a third parameter must be introduced, and one candidate is of course the Ma number, $Ma=|\mathbf{v}|/c_R$, evaluated at a reference temperature T_R. However, a more appropriate quantity is the ratio between the temperature rise associated with the kinetic energy, ΔT_S, and the temperature rise due to the chemical reactions, occurring at constant pressure, ΔT_C, i.e. $S=\Delta T_S/\Delta T_C$. The temperature rise associated with the kinetic energy can be estimated as $\Delta T_S \approx \frac{1}{2}(\gamma-1)Ma^2 T_R$, whereas the temperature rise due to the chemical reactions can be related to the Zel'dovich number $\beta=\Delta T_C T_A/T_R^2$, where T_A is the activation temperature. Accordingly, $S=\frac{1}{2}(\gamma-1)Ma^2 T_R/\Delta T_C$. Hence, for low speed flows $S<<1$ and the kinetic energy is small compared to the chemically stored energy, when $S\approx 1$ the two energy levels are equal, but when $S>>1$ the kinetic energy of the reactants dominates. The typical values of $\beta>>1$ lead to the special features of low speed turbulent combustion in the reaction sheet regime, features that are expected to persist in high-speed flows until ΔT_S is comparable with ΔT_C. Hence, if $Ma<\sqrt{2/(\gamma-1)\cdot T_R/T_A}$ temperature changes due to compressibility have negligible effect on the chemical kinetics since $\beta S<<1$; if $\sqrt{2/(\gamma-1)\cdot T_R/T_A}<Ma<1$ temperature changes due to compressibility may influence the chemical kinetics and the exothermicity, but eddy shocklets do not occur; if $1<Ma<\sqrt{2/(\gamma-1)\cdot \Delta T_C/T_R}$ eddy shocklets and expansion waves form, but the temperature change, and the reaction rate changes produced by compressibility remain less than those resulting from heat release; and if $Ma>\sqrt{2/(\gamma-1)\cdot \Delta T_C/T_R}$ temperature changes from compressibility are larger than those from the heat release, and shocklets may occur.

4.3. Turbulence Modeling

As already discussed in Section 4.1 the direct numerical simulation of scramjet flows (and most turbulent flows of practical or engineering interest) will require too fine computational meshes for present-day computers to handle. Direct Numerical Simulations (DNS), in which all spatial and temporal scales of relevance are fully resolved, may however still be useful for investigating building-block flows in simple configurations in order to gain additional insight in the physics and the chemistry, and their mutual interactions.

The most common turbulence modeling approach is the Reynolds Averaged Navier-Stokes (RANS) models, which is based on a statistical treatment of the fluctuations about a stationary or a very slowly varying flow, [32]. The dependent variables $\{\rho, \mathbf{v}, e, Y_i\}$ are broken into two parts: a mean, time- or ensemble-averaged part of the flow and a fluctuating component representing deviations from this mean. This approach is only formally correct in the limit of stationary mean flow otherwise the mean and fluctuating parts cannot be cleanly separated. The governing RANS equations follow from taking the mean value of (3) and (4), and the resulting equations are of the same form, but with some additional terms describing the mean influence of the fluctuations on the mean flow. For a non-reacting flow (no Y_i-equations) these terms consist of the Reynolds stress and flux terms (in the momentum and energy equations respectively) and the turbulent dissipation term in the energy equation. These terms must be modeled in order to close the equations, and a variety of turbulent closure models exist. The simplest consists of two-equation eddy

viscosity models, whereby the Reynolds stress and flux terms are assumed proportional to the rate-of-strain and temperature gradients, respectively, the proportionality constants being the turbulent viscosity and the turbulent heat conduction, respectively, [33]. These quantities are then estimated from the turbulent kinetic energy and its dissipation rate. The most advanced models consist of modeled transport equations for the Reynolds stress and flux terms, in which a number of terms are parameterized in different ways, [34]. The advantage of the RANS approach is that it is fast (since only the mean flow is sought) and it is readily available in most commercial CFD codes, and it is streamlined to handle unstructured complex meshes. The main drawback is that all turbulent flows are unsteady, and it is virtually impossible to obtain any detailed information of such a flow from its mean flow. This is particularly true for combusting flows in which turbulence and chemical reactions interact. For such flows additional terms that have to be modeled appear: a Reynolds flux term and a mean reaction rate. Although the Reynolds flux term can be modeled in the same way as its counterpart in the energy equation, the mean reaction rate is more difficult to handle as will be discussed in Sections 4.4.

A promising alternative to RANS for flows of technological interest is Large Eddy Simulation (LES). In LES, all scales larger than the mesh are resolved using a space and time accurate scheme and only the small scales are modeled using a subgrid model that is considered relatively universal. The direct computation of the large, energy containing eddies (which are geometry and flow dependent features) gives LES more generality than the RANS method, which models the entire spectrum of turbulent motions. The computational cost of LES, although significant is fast becoming reasonable with the advent of massively parallel computers. Although applications of LES to subsonic non-reacting and reacting flows have been reported, application to supersonic and/or hypersonic flows has been limited so far. In particular, LES of scramjet flow field will require not only accurate simulation of the large-scale features determined by the engine design but also of the small-scale mixing process that dominates fuel-air mixing and combustion process. After splitting the dependent variables $\{\rho, \mathbf{v}, E, Y_i\}$ into resolved (denoted by an overbar or a tilde) and unresolved components, the governing equations (3) and (4) are low-pass filtered to obtain equations for $\{\overline{\rho}, \tilde{\mathbf{v}}, \tilde{E}, \tilde{Y}_i\}$. More precisely, following [35],

$$\begin{cases} \partial_t(\overline{\rho})+\nabla\cdot(\overline{\rho}\tilde{\mathbf{v}})=0, \\ \partial_t(\overline{\rho}\tilde{Y}_i)+\nabla\cdot(\overline{\rho}\tilde{\mathbf{v}}\tilde{Y}_i)=\nabla\cdot(\overline{\mathbf{j}_i}-\mathbf{b}_i)+\overline{\dot{w}_i}, \\ \partial_t(\overline{\rho}\tilde{\mathbf{v}})+\nabla\cdot(\overline{\rho}\tilde{\mathbf{v}}\otimes\tilde{\mathbf{v}})=-\nabla\overline{p}+\nabla\cdot(\overline{\mathbf{S}}-\mathbf{B})+\overline{\rho}\tilde{\mathbf{f}}, \\ \partial_t(\overline{\rho}\tilde{E})+\nabla\cdot(\overline{\rho}\tilde{\mathbf{v}}\tilde{E})=\nabla\cdot((-\overline{p}\mathbf{I}+\tilde{\mathbf{S}})\tilde{\mathbf{v}})+\nabla\cdot(\overline{\mathbf{h}}-\mathbf{b})+\overline{\rho}\varepsilon+\overline{\rho}\tilde{\sigma}, \end{cases} \qquad i=1,\ldots,N, \tag{6}$$

where $\mathbf{B}=(\overline{\rho\mathbf{v}\otimes\mathbf{v}}-\overline{\rho}\tilde{\mathbf{v}}\otimes\tilde{\mathbf{v}})$, $\mathbf{b}=(\overline{\rho\mathbf{v}E}-\overline{\rho}\tilde{\mathbf{v}}\tilde{E})$, $\mathbf{b}_i=(\overline{\rho\mathbf{v}Y_i}-\overline{\rho}\tilde{\mathbf{v}}\tilde{Y}_i)$ and ε are the subgrid scale stress, flux and dissipation terms, respectively; $\overline{\mathbf{j}_i}=\overline{D_i\nabla Y_i}$, $\overline{\mathbf{S}}=\overline{(\lambda+\frac{2}{3}\mu)(\mathrm{tr}\mathbf{D})\mathbf{I}+2\mu\mathbf{D}_D}$ and $\overline{\mathbf{h}}=\overline{\kappa\nabla T}$ are the low-pass filtered constitutive equations; $\tilde{E}=\overline{\rho(e+\frac{1}{2}\mathbf{v}^2)}/\overline{\rho}=\overline{\rho(h-p/\rho+\frac{1}{2}\mathbf{v}^2)}/\overline{\rho}$ and $\overline{p}=\overline{\rho RT\sum_i(Y_i/M_i)}$ are the low-pass filtered state equations, and,

$$\overline{\dot{w}_i}=\sum_{j=1}^{M}(P_{ij}''-P_{ij}')\overline{\dot{w}_{ij}}=\sum_{j=1}^{M}(P_{ij}''-P_{ij}')\left[\tilde{k}_{fj}\overline{\rho}^{\sum_i P_{ij}'}\prod_{i=1}^{N}\tilde{Y}_i^{P_{ij}'}-\tilde{k}_{bj}\overline{\rho}^{\sum_i P_{ij}'}\prod_{i=1}^{N}\tilde{Y}_i^{P_{ij}''}+\dot{w}_{ij}^{sgs}\right]=\sum_{j=1}^{M}(P_{ij}''-P_{ij}')\left[\dot{w}_{ij}^{gs}+\dot{w}_{ij}^{sgs}\right], \tag{7}$$

are the filtered reaction rates, where $\dot{w}_{ij}^{sgs}$ is the subgrid reaction rate contribution. To close the reactive LES equations (6), subgrid models are thus required for:

- the subgrid stress, flux and dissipation terms, which are not unique to reacting flows and hence models developed for non-reacting flows may be used. The most common model is

the subgrid viscosity approach, $\mathbf{B}=\frac{2}{3}(\overline{\rho}k-\mu_k\nabla\cdot\tilde{\mathbf{v}})\mathbf{I}-2\mu_k\tilde{\mathbf{D}}_D$, [36], in which the subgrid kinetic energy, k, and the subgrid viscosity, μ_k, are obtained from models like the Smagorinsky (SMG) model, [36], $k=c_I\Delta^2\|\tilde{\mathbf{D}}\|^2$ and $\mu_k=c_D\Delta^2\overline{\rho}\|\tilde{\mathbf{D}}\|$, that will be used here. The subgrid flux vector terms ($\mathbf{b}_i$ and $\mathbf{b}$) are handled similarly, e.g. $\mathbf{b}=-(\mu_k/\overline{C}_P)\nabla\tilde{E}$, etc.;

- the filtered (non-linear) state and constitutive equations which are usually simplified by assuming that the subgrid temperature and species fluctuations can be neglected. This results in the simplified state equations $\tilde{E}=\tilde{h}-\overline{p}/\tilde{\rho}+\frac{1}{2}\tilde{\mathbf{v}}^2$ and $\overline{p}\approx\overline{\rho}R\tilde{T}\sum_i(\tilde{Y}_i/M_i)$, and the constitutive equations $\overline{\mathbf{S}}\approx(\tilde{\lambda}+\frac{2}{3}\tilde{\mu})(\mathrm{tr}\tilde{\mathbf{D}})\mathbf{I}+2\tilde{\mu}\tilde{\mathbf{D}}_D$, $\overline{\mathbf{j}}_i\approx\tilde{D}_i\nabla\tilde{Y}_i$ and $\overline{\mathbf{h}}\approx\tilde{\kappa}\nabla\tilde{T}$, respectively.
- the (non-linear) subgrid reaction rate contribution $\dot{w}_{ij}^{sgs}$, will be most difficult to model due to the combined effects of species and temperature fluctuations. Neglecting subgrid temperature and species fluctuations is consistent with the above assumption but may result in incorrect predictions of the turbulent flame speed since the chemical reactions mainly occur on the subgrid space and time scales.

4.4. Combustion Modeling

The combustion chemistry enters the problem of turbulent reacting flows trough the thermodynamics and the reaction rates $\dot{w}_{ij}$, as discussed in Section 4.3. Moreover, the accuracy and detail of the combustion chemistry is set by the reaction mechanism – a detailed reaction mechanism is usually more accurate than a global or reduced mechanism, but also much more complicated and expensive to handle in a CFD simulation. This is due to the fact that more equations have to be solved for a detailed reaction mechanism, and that the non-linearity of these equations makes it more difficult to obtain a stable solution. Another reason for not using detailed reaction mechanisms is that it is difficult to obtain correct values for the rate parameters. For turbulent combustion, using RANS or LES, the mean reaction rates have to be modeled – a very difficult issue due to the non-linear behavior of these equations. Because of these problems other approaches to describe the chemical reactions and the exothermicity are sought for.

In LES more details of the flow and thermodynamics is available which somewhat simplifies the combustion modeling problem when compared to RANS. At present, there are four main routes to combustion modeling in LES, [37], and these are:

- Reduced or global reaction mechanisms (typically involving two to four reaction steps) with Arrhenius rate expressions in which the species and temperature fluctuations usually are neglected. High-resolution non-oscillatory algorithms are often used to circumvent the numerical problems associated with thin flame fronts, e.g. [38].
- Flamelet models in which the reaction is assumed to take place in thin layers, separating fresh gases from burnt products being wrinkled by the turbulence. These models are based on a non-reactive scalar (the mixture fraction) and a reactive scalar (a reaction coordinate) together with models for the laminar flame speed, S_u that can be obtained from a detailed reaction mechanism, and the influence of the subgrid turbulence, [39].
- Transported or presumed Probability Density Function (PDF) models using analytical or transported PDFs to close either the filtered species equations (6_2) or a flamelet library that is derived from solutions to (6_2) under idealized conditions. The flamelet library is usually parameterized by a non-reactive scalar and its variance, [40].
- Linear Eddy Modelling using a grid-within-the-grid approach to solve 1D equations (based

on Arrhenius chemistry) with sufficient resolution, [41].

At present it is not clear which approach is the best – all methods have merits and demerits – but in this study we focus on the flamelet library approach due to its simplicity. Following Burke-Schumann, [42], the species concentrations are primarily assumed to be functions of the mixture fraction, z, i.e. $Y_i=\hat{Y}_i(z)$, but also other parameters may be used to parameterize the species mass fractions. For turbulent flames, the scalar dissipation rate, χ, which takes flame stretch and local quenching into account is appropriate to consider, such that $Y_i=\hat{Y}_i(z,\chi)$. The flamelet library now contains information about the detailed structure of the flame, provided z and χ. In LES, however, it is sufficient to incorporate only the large scale, resolvable, structure of the flame, which, given a flamelet library of the form $\hat{Y}_i(z,\chi)$, may be reconstructed from,

$$\tilde{Y}_i=\int_0^1\int_0^\infty \hat{Y}_i(z,\chi)\wp(z,\chi,\tilde{z},\tilde{\chi})dzd\chi, \tag{8}$$

where $\wp=\wp(z,\chi,\tilde{z},\tilde{\chi})$ is the subgrid PDF. In the integrand of (8) the first term represents the intrinsic flame structure, whereas the PDF relates to the modelling of the subgrid mixing. The PDF $\wp$ is now a joint PDF of z and χ which is rather difficult to handle, and instead it is commonly assumed that z and χ are uncorrelated so that $\wp(z,\chi,\tilde{z},\tilde{\chi})=\wp_z(z,\tilde{z})\wp_\chi(\chi,\tilde{\chi})$ and moreover we assume that the effects of the subgrid fluctuations in χ are small so that $\wp(z,\chi,\tilde{z},\tilde{\chi})=\wp_z(z,\tilde{z})\delta(\chi-\tilde{\chi})$, where δ is the Dirac function, such that $\tilde{Y}_i=\int_0^1\hat{Y}_i(z,\tilde{\chi})\wp_z(z,\tilde{z})dz$. It now remains to determine the shape of the PDF of the mixture fraction. In principle, this can be done by solving a transport equation for $\wp_z$, using Monte Carlo techniques, but this is far too expensive, and instead we have adopted the method of presumed PDF's, which amounts to specifying the PDF analytically beforehand. The most common PDF is the β-function, in which $\wp_z$ is approximated by the β-function, [43], that is parameterized in terms of z and its variance $\tilde{z}''^2$, i.e.,

$$\wp_z(z,\tilde{z})=z^{a-1}(a-z)^{b-1}/\Gamma,\ \text{where}\ \Gamma=\int_0^1(z'^{a-1}(a-z')^{b-1})dz', \tag{9}$$

where $a=\tilde{z}(\tilde{z}(1-\tilde{z})/\tilde{z}''^2-1)$ and $b=a/\tilde{z}-a$. The low-pass filtered mixture fraction, $\tilde{z}$, is obtained from the low-pass filtered and partially modeled transport equation,

$$\partial_t(\bar{\rho}\tilde{z})+\nabla\cdot(\bar{\rho}\tilde{\mathbf{v}}\tilde{z})=\nabla\cdot(D_z\nabla\tilde{z}-\mathbf{b}_z),\ \ \mathbf{b}_z=-\mu_k\nabla\tilde{z}, \tag{10}$$

whereas its variance is obtained from the analytical expression $\tilde{z}''^2=c_C\Delta^2|\nabla\tilde{z}|^2$, with $c_C=0.065$, in accordance with how the subgrid kinetic energy, k, is estimated as $k=c_I\Delta^2\|\tilde{\mathbf{D}}\|^2$, with $c_I=0.133$. In addition, the scalar dissipation rate of variance of the mixture fraction, $\tilde{z}''^2$, is then modelled as $\tilde{\chi}=2\tilde{z}''^2\sqrt{k}/\Delta=2c_Cc_I^{1/2}\Delta^2|\nabla\tilde{z}|^2\|\tilde{\mathbf{D}}\|$. The flamelet library, used in this study to calculate the mass fractions $\tilde{Y}_i$, involves five species (H_2, O_2, OH, H_2O and N_2), [44], and is tabulated for different values of z and χ. Finally, the temperature is calculated from the solution of the energy equation using the caloric equation-of-state involving the $\tilde{Y}_i$'s from the flamelet library.

4.5. Numerical Methods for Supersonic Flows

The governing equations of the reactive flow model described in Sections 4.2 and 4.3 are discretized using an unstructured Finite Volume (FV) method, [45]. The use of unstructured meshes greatly facilitates meshing of complex geometries, although not utilized here. The spatial discretization is based on Gauss theorem, [46], whereby the partial differential equations of the model,

(6_1), (6_3), (6_4) and (10), are converted into a set of discrete equations,

$$\partial_t(\mathbf{U}_P)+\tfrac{1}{\delta V_P}\textstyle\sum_f\left[\mathbf{F}_f(\mathbf{U})\right]=\mathbf{s}(\mathbf{U}_P), \tag{11}$$

where $\mathbf{U}=[\overline{\rho},\overline{\rho}\tilde{z},\overline{\rho}\tilde{\mathbf{v}},\overline{\rho}\tilde{E}]$ is the vector of conserved variables, $\mathbf{F}(\mathbf{U})$ the corresponding flux tensor, and $\mathbf{s}(\mathbf{U})$ the source vector. Moreover, δV_P is the control volume of the P^{th} cell and f denotes the cell faces over which all fluxes are integrated. The convective fluxes are reconstructed using the values of the neighboring control volumes using a flux limiting approach in which

$$\begin{aligned}\mathbf{F}_f^C(\mathbf{U})&=\mathbf{F}_f^{C,H}(\mathbf{U})-(1-\Psi)\left[\mathbf{F}_f^{C,H}(\mathbf{U})-\mathbf{F}_f^{C,L}(\mathbf{U})\right]\\&=|\mathbf{F}_f^C(\mathbf{U})|\left[\left(\beta^+ +\Psi(\ell_f\,\mathrm{sgn}(F_f^C)-\beta^+)\right)\mathbf{U}_P+\left(\beta^- +\Psi((1-\ell_f)\mathrm{sgn}(F_f^C)-\beta^-)\right)\mathbf{U}_N\right],\end{aligned} \tag{12}$$

where $\beta_f^{\pm}=\frac{1}{2}(\mathrm{sign}(\mathbf{F}_f^C(\mathbf{U}))\pm 1)$, ℓ_f the distance between opposing faces, and Ψ the flux limiter that guarantees second order accurate and smooth reconstruction even for solution fields with large local variations. Here, a Total Variational Diminishing (TVD) compatible flux limiter, the Van Leer limiter, [47], is used. The diffusive fluxes are reconstructed using central differencing of the inner derivatives such that $\mathbf{F}_f^D(\mathbf{U})=\mu|d\mathbf{A}_f|(\mathbf{U}_N-\mathbf{U}_P)/|\mathbf{d}_f|$, where μ is the viscosity, $d\mathbf{A}_f$ the area of face f and $\mathbf{d}_f$ the inter-cell distance. The discrete equations are finally integrated in time using a second order accurate TVD compatible Runge-Kutta scheme, [48],

$$\begin{cases}\mathbf{U}^*=\mathbf{U}^n-\Delta t\left(\frac{1}{\delta V_P}\sum_f\left[\mathbf{F}_f(\mathbf{U}^n)\right]-\mathbf{s}(\mathbf{U}_P^n)\right),\\ \mathbf{U}^{n+1}=\frac{1}{2}(\mathbf{U}^n+\mathbf{U}^*)-\frac{1}{2}\Delta t\left(\frac{1}{\delta V_P}\sum_f\left[\mathbf{F}_f(\mathbf{U}^*)\right]-\mathbf{s}(\mathbf{U}_P{}^*)\right),\end{cases} \tag{13}$$

where Δt is the time-step. The algorithm (13) is stable for Courant numbers, $Co=|\mathbf{v}\pm c|\Delta t/\Delta x$, of less than 1, where $c=\sqrt{\gamma RT}$ is the local speed of sound and $\gamma=\overline{C}_P/\overline{C}_V$. The fact that Co depends on c, which is a function of T, has important practical consequences when simulating high-speed combustion. Since the chemical reactions are exothermal, the local speed of sound is increased, which together with the requirement that $Co<1$ implies that a smaller Δt must be used as compared a corresponding non-reacting flow. Hence, a reacting (exothermal) process is considerably more expensive to simulate than a non-reactive flow. Moreover, since we resolve the dynamics of the large scale flow structures a Co number less than 0.5 is used.

5. The DLR Scramjet Experimental Rig

A schematic of the scramjet experimental facility, [49-52], is presented in figure 6. Preheated air is expanded through a laval nozzle, and enters the combustor section at Ma=2.0. The combustor has a width of 40 mm and a height of 50 mm at the entrance and a divergence angle of the upper channel wall of three degrees to compensate for the expansion of the boundary layer. A wedge shaped strut is placed in the center of the combustion chamber downstream of the nozzle. Just downstream of the laval nozzle the height of the 32 mm long strut is 6 mm. Along the first 100 mm downstream of the laval nozzle, the side walls and the upper wall are made from quartz glass to allow optical access and to minimize the reflection of scattered light on the wall opposite the observation window. Hydrogen (H_2) is injected at Ma=1.0 through a row of 15 holes in the strut base, having a diameter of D=1.0 mm and a distance between adjacent holes of 2.4 mm.

Typical mass flows in the experiments, [49-52], were varied between 1.0 kg/s and 1.5 kg/s for the air and between 1.5 g/s and 4.0 g/s for hydrogen. In the present study we focus on a case with a hydrogen jet velocity of v_J=1200 m/s and an airstream velocity of v_A=730 m/s, corresponding to mass flows of about 1.0 g/s for the hydrogen jet and 1.0 kg/s for the air, given the densities ρ_{H2}=0.097 kg/m^3 and ρ_{air}=1.002 kg/m^3. The hydrogen is injected at ambient temperature and pressure, i.e. at T_J=250 K and p_J=10^5 Pa, whereas the air was injected at T_A=340 K at at p_A=10^5 Pa, respectively. Combustion was initiated by pre-burning of a small amount of O_2 in a H_2 tube by a spark, which was turned off after ignition. A wide range of measurements were conducted in this rig, including LDV and PIV measurements of the velocity, CARS measurements of the temperature, OH-LIF for mapping regions of combustion as well as more conventional schlieren and shadow photography in order to characterize the flow and combustion dynamics.

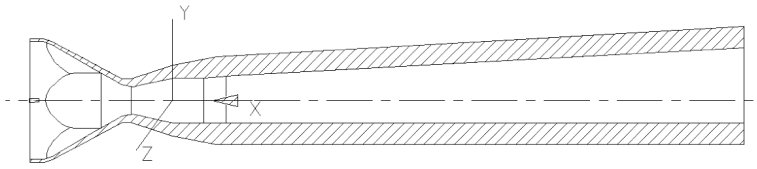

Figure 6. Schematic overview of the DLR scramjet rig.

The computational configuration is simplified in the sense that instead of modeling the full width of the combustor, including the 15 injector holes and the side walls, a smaller domain with three injector holes and periodic boundary conditions in the spanwise (or z) direction was chosen as the computational domain, see figure 7a. The reason for this simplification is that we wish to reduce the computational cost as much as possible, but still retaining all relevant physics of the scramjet combustor. Two computational grids have been fabricated (see figure 7b) with 1.5 and 3.0 million control volumes, respectively. The grid is block structured, using only hexahedral elements, divided into 12 blocks per jet. The first grid point is located at a normalized wall distance of $y^+\approx$50 in order to make maximum use of the subgrid wall model, [53], employed to alleviate some of the requirements for resolving the near wall boundary layer.

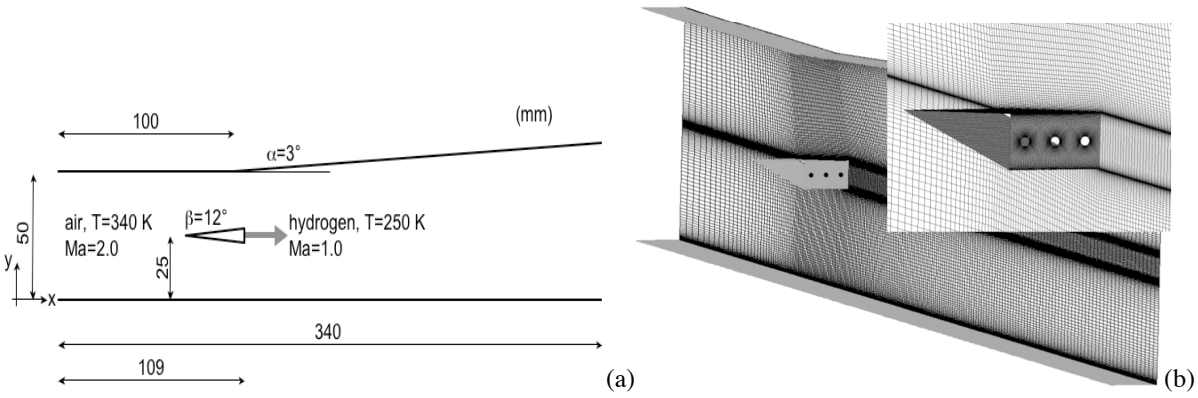

Figure 7. (a) Schematic of the computational domain and (b) the computational grid used here.

According to the theory of characteristics, all variables are prescribed at the inlet and at the hydrogen jets at the base of the strut, i.e. Dirichlet boundary conditions, whereas all variables are extrapolated at the outlet, i.e. zero Neumann boundary conditions. Periodic boundary conditions, 10 mm apart, are used in the spanwise direction. At the upper, lower and strut walls, no-slip conditions are applied to the velocity whereas zero Neumann conditions are applied to all other vari-

ables. Subgrid wall-models, based on the logarithmic law-of-the-wall, [53], in which μ_k is modified for the flow to satisfy a logarithmic velocity distribution, are used to handle the near-wall resolution problem. The computations are initialized with the state of the incoming air, and are continued until the second order statistical moments have converged.

6. Computational Results

In this section we describe the results from the numerical simulations of (i) the flow in the combustion chamber without hydrogen injection and combustion, (ii) the flow in the combustion chamber with hydrogen injection but without combustion, and finally (iii) the flow in the combustion chamber with hydrogen injection and combustion. For each grid, the simulations are started in sequence in order to take advantage of the successive development of the flow. The initial conditions consist of a uniform flow of 730 m/s, corresponding to a Ma number of 2 in air, a uniform pressure of 10^5 Pa and a uniform temperature of 340 K. Here we will focus on the LES results from the finer grid, consisting of about 3.0 million cells, since the spatial resolution is imperative for capturing the dynamics of the shocks, expansion fans and the possibly reacting shear layers, and their mutual interactions that are important for this case.

6.1. Supersonic Flow without Hydrogen Injection and Combustion

The first test case involves the flow only, i.e. the hydrogen injection and the subsequent combustion are turned off. This test case, hereafter referred to as Case I, will serve the principle purpose of helping us to characterize the flow in the combustion chamber, and since experimental data is available, it will also aid in validating the LES model and the supersonic flow code that will be used also for the other two cases. The measurements carried out for Case I in the experimental facility are however limited to schlieren photographs and time-averaged pressure data at the bottom wall. The absence of velocity measurements, as available for the other cases, will not affect the overall judgment of the code and model performance, nor the understanding of the different processes involved in the combustor operation since the experimental schlieren and shadowgraph photographs hold sufficient information for comparison with the LES.

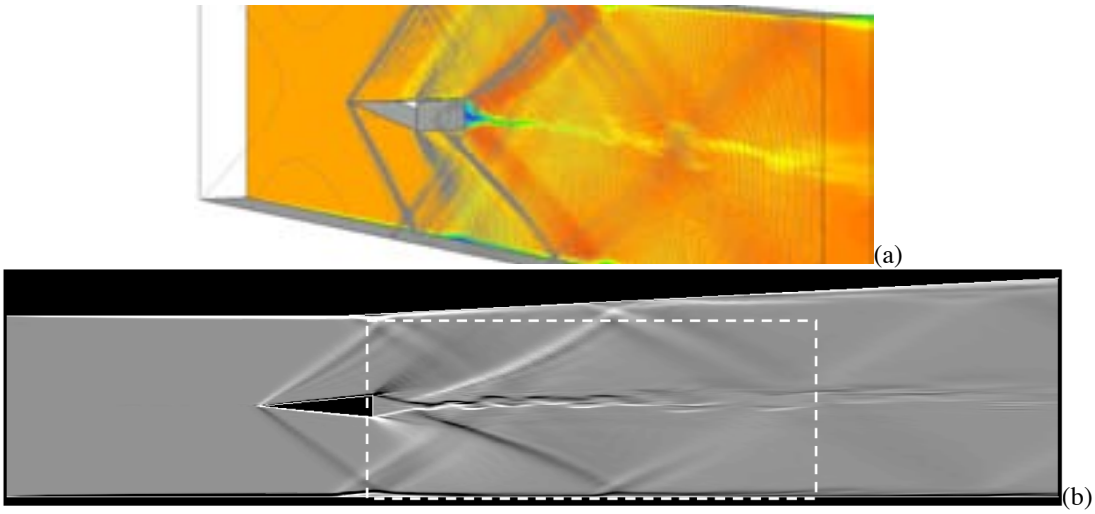

Figure 8. Results from Case I involving supersonic flow in the scramjet combustor but without hydrogen injection and combustion. (a) Perspective view from the rear of the simulated flow in terms of velocity and pressure contours and (b) a numerical schlieren image from the LES.

Schlieren imaging measures the deflection of the optical path-length, $\ell=\int_S n(\mathbf{x}(s))ds$, where n is the refractive index and $\mathbf{x}=\mathbf{x}(s)$ is the path in parametric form, when a light ray is transmitted through an inhomogeneous medium with a varying n. For a gaseous mixture n can be estimated by the Lorentz-Lorenz formula $(n^2+1)\rho\sum_i Y_i A_i=\overline{M}(n^2-1)$, where $\overline{M}$ is the molecular weight of the mixture and A_i the molar refractivity for specie i. In the experiments the schlieren images are obtained by using a horisontal knife-edge that cuts off light propagating in the vertical (i.e. the y direction), and for small devations along the optical path, i.e. for small variations in n, the intensity variations in the schlieren image are $\Delta I\propto\int_0^{L_z}(\nabla_y n)dz$. Similarly, for small variations in the refractive index, shadowgraph images, measuring the radius of curvature of the optical path-length, can be obtained from n as $\Delta I\propto\int_0^{L_z}(\nabla\cdot(\nabla n))dz$. In this report, we use the LES data to calculate the refractive index from Lorentz-Lorenz formula as $n=\sqrt{(1+2\alpha)/(1-\alpha)}$, where $\alpha=p\sum_i(Y_i A_i)/(R_0 T)$, from which both numerical schlieren and shadowgraph images can be reconstructed and subsequently compared with experimental light deflection images.

In figure 8 the flow is from left to right, and the wedge, at the base of which hydrogen can be injected parallel into the air-stream is clearly visible. The dashed box just behind the wedge denotes the region in which the experimental schlieren images have been recorded, and the resemblence with the experimental schlieren image (figure 4a in [51]) is very good. An oblique shock is formed at the tip of the wedge, which reflects off the upper and lower walls of the combustion chamber downstream of the recirculation bubble behind the wedge. This causes a characteristic shock pattern in the downstream region of the combustor on which the asymmetry is not noticed. At the upper and lower walls, the boundary layer is strongly affected, at least locally, by the reflections of this oblique shock. These local modifications involve thickening of the boundary layer, higher rms-pressure fluctuations and elevated wall temperatures. The boundary layer on the wedge surface separates at the base and a shear layer is formed. This shear layer is naturally unstable and is therefore prone to break-up and develop into Kelvin-Helmholtz structures. However, before this process is completed, the reflections from the oblique shock at the tip of the wedge have started to interact with the shear layer, causing it to bend and to distort, forming ondulating large-scale structures. Without hydrogen injection strong expansion fans at the upper and lower corners of the wedge rapidly deflect the flow towards the centerline. Furthermore, a small, triangular-shaped recirculation bubble is formed just downstream of the base of the wedge associated with low base pressure and recompression shocks. Estimates of the oblique shock angle show very good agreement with the experimental data. After some distance the flow in the wake of the wedge is accelerated back to supersonic speeds, and the subsequent shocks (reflecting off the walls) passes through the accelerating wake.

6.2. Supersonic Flow and Mixing with Hydrogen Injection

Inert hydrogen injection adds significant complexity to the flow in the scramjet combustor since hydrogen has a considerably lower molar mass (M_{H2}=2 g/mol) than air (M_{air}=29 g/mol), which makes mixing an important process in establishing the conditions for scramjet combustion. In order to examine supersonic mixing separately we next simulate a case, hereafter referred to as Case II, in which hydrogen is injected through holes in the rear end of the wedge shaped flame holder. This simulation is restarted from the results obtained in Case I in order to save computer time. Detailed experimental results are available from DLR for this case, and consist of schlieren photographs, planar ultra-violet Rayleigh scattering images and Particle Image Displacement Velocimetry (PIV) measurements on the centerline vertical plane, and side-wall pressure measure-

ments as well as Laser Doppler Velocimetry (LDV) measurements at four vertical lines downstream of the wedge and on the combustor centerline. Schlieren and Rayleigh scattering images gives qualitative information only, but on a plane, whereas LDV and side-wall pressure measurements gives quantitative information about the velocity and pressure, respectively, along discrete lines through the flow. PIV gives information on the velocity field on a plane, but with less accuracy than LDV. The measurement data is sufficient to validate the flow and mixing model and to extract detailed information about the flow and mixing process.

Figure 9 shows experimental and numerical schlieren photographs as well as a perspective view from the rear, in terms of velocity, H_2 concentration and pressure of Case II. With hydrogen injection the flow field is similar to that of Case I but with a few differences: (i) the expansion fan coming off the base of the wedge is not as strong due to the presence of hydrogen that affects the thermodynamic properties of the fluid; (ii) the recirculation region is now much larger with a somewhat higher base pressure; (iii) the curved recompression shocks of Case I are here replaced with straighter recompression shocks; (iv) the shear layers, originating at the upper and lower corners of the wedge, are now clearly visible due to the different thermodynamic properties of the wake in Case II as compared to Case I. The hydrogen rich stream is clearly visible, in particular where the shock crosses the core flow and where the shock angle is increased. For the shear layers, we find that the strength of the gradient between the hydrogen and the air decreases with distance from the wedge due to the effects of the mixing. The shear layers are unstable due to Kelvin-Helmholtz (KH) instabilities. Because of the one-sided divergent channel the upper reflecting shock hits the hydrogen filled wake further downstream than the lower shock causing an asymmetric flow field in which the KH modes are amplified. This in turn results in shedding and periodically bent structures whereby air and hydrogen are mixed by advection – a process much more effective than diffusion. It is important also to notice that compressibility leads to reduced shear layer growth affecting the formation and subsequent break-up of large coherent structures. In addition, the reflected shock waves are deflected by the hydrogen jets. The agreement with the experimental schlieren image (figure 4b in [51]) is good, suggesting that LES can differentiate between the curved recompression shocks observed in Case I and the straighter recompression shocks found in Case II, which are due to the hydrogen injection.

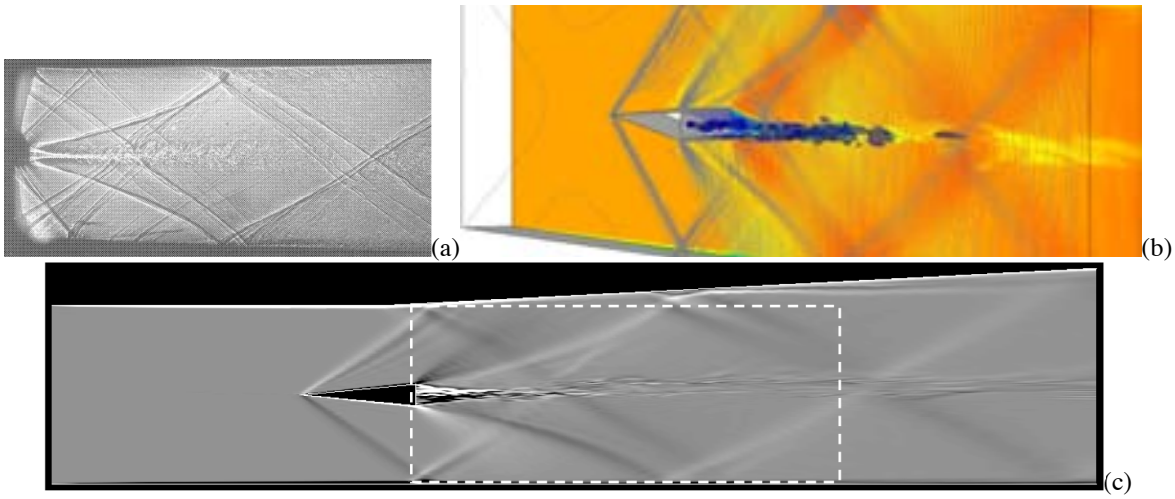

Figure 9. Results from Case II involving supersonic flow in the scramjet combustor with hydrogen injection but no combustion. (a) Schlieren photographs from the experiments, [49], (b) a perspective view from the rear of the simulated flow, and (c) a numerical schlieren image from the non-reacting LES calculations. The size and location of the experimental image (a) is superimposed on (c).

In the experiments, mixing is studied by Rayleigh scattering, [52], which is a non-intrusive measurement technique based on elastic scattering. Elastic scattering can easiest be explained by regarding the molecule as a dipole (the positive nuclei and the electrons are separated by the incident electromagnetic field) that starts to oscillate with the same frequency as the incident light. The molecule will then work as a point antenna, spreading radiation in all directions. Rayleigh scattering occurs for small particles, with sizes much smaller than the light wavelength, e.g. molecules, while Mie scattering occurs for larger particles, [54]. Different molecules (or species) have different Rayleigh-scattering cross section, and images can be obtained via a CCD camera. Using the LES data, Rayleigh scattering images can be estimated from the power of the scattered light, which according to Eckbreth, [54], is $P_{ray} \propto (n-1)^2/\rho$, where n is the refractive index. Both the experimental Rayleigh scattering images (figure 4 in [52]) and the numerical estimates in figure 10, shows the recompression shocks due to the density jump across the shock wave. In the core of the combustor the distribution is visible as a dark region due to the smaller Rayleigh-scattering cross section of the fuel in comparison to the Rayleigh-scattering cross section of air. Just behind the wedge a nearly homogeneous hydrogen region, with a slightly convergent shape is observed. Further downstream, the contour of the flow-field becomes more ragged with larger structures and large-scale air entrainment into the mixing region. The mixing mechanism is very important for the supersonic combustion process, and convective mixing is known to reduce the growth rate of the shear layers, [55], resulting in less efficient mixing.

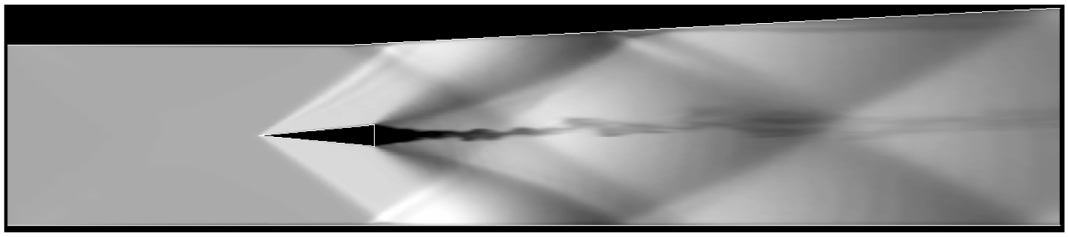

Figure 10. Results from Case II involving supersonic flow in the scramjet combustor with hydrogen injection but no combustion. Numerical estimates of the Rayleigh scattering.

In figure 11 we compare the predicted and experimentally measured pressure at the lower wall and the axial velocity distribution and its rms fluctuations at four cross-sections downstream of the wedge. For the time-averaged pressure $\langle \overline{p} \rangle$ in 11a, with the time-averaging carried out over 4 flow-through times, we find reasonable qualitative agreement. In the LES, the reflection of the leading edge shock is well predicted both with respect to position and amplitude. Furthermore, the amplitude of $\langle \overline{p} \rangle$ in the LES computations is somewhat under-predicted and the reason for this is believed to be the lack of spatial resolution in this region of the combustor. For the time-averaged axial velocity $\langle \tilde{v} \rangle_x$ in 11b, the overall agreement is good. In particular we find that the LES can predict the recovery of the subsonic hydrogen jet forming the wake reasonably well. Just after the jet exits the wedge it is accelerated in the low-pressure recirculation region followed by a deceleration by a shock wave. After further acceleration the hydrogen jet is well mixed with the ambient air and has reached a nearly constant velocity of 760 m/s, which is in good agreement with the experimental data. Moreover, the influence of the hydrogen jet on the flow limited to the region in the immediate vicinity of the jets and only very small differences between Case I and Case II can be detected in the velocity field. For the axial rms-velocity fluctuations, $v_x^{rms} = \sqrt{\langle \tilde{v}_x - \langle \tilde{v}_x \rangle \rangle^2}$, we find high values in the wake, and around the jet, which however decrease with downstream distance. Also, high values are found close to the upper and lower

walls, which are associated with the near-wall production of turbulence emulated by the wall-model. Comparison with data at x/h= 22.54 and 28.36 show good agreement.

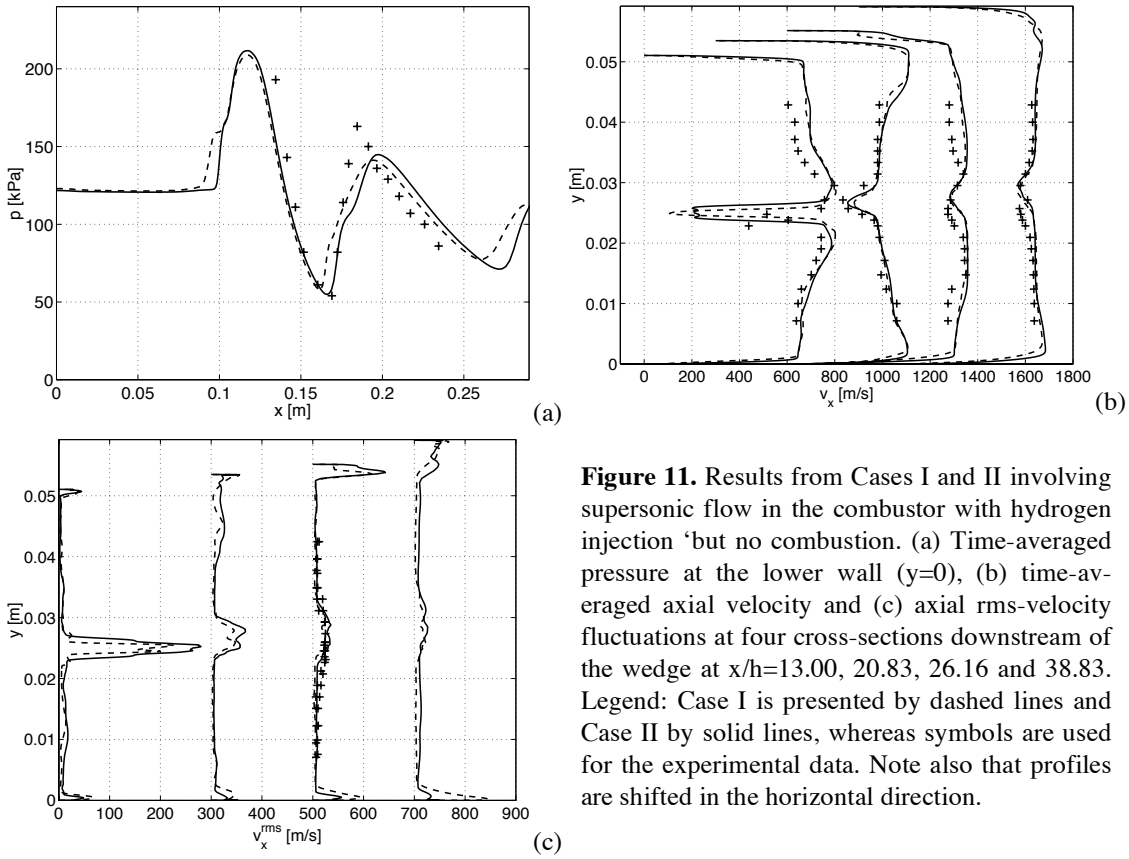

Figure 11. Results from Cases I and II involving supersonic flow in the combustor with hydrogen injection 'but no combustion. (a) Time-averaged pressure at the lower wall (y=0), (b) time-averaged axial velocity and (c) axial rms-velocity fluctuations at four cross-sections downstream of the wedge at x/h=13.00, 20.83, 26.16 and 38.83. Legend: Case I is presented by dashed lines and Case II by solid lines, whereas symbols are used for the experimental data. Note also that profiles are shifted in the horizontal direction.

6.3. Supersonic Mixing and Combustion

In order to examine supersonic combustion we next study Case III, in which hydrogen is injected through holes in the rear end of the wedge-shaped flame holder, forming a combustible mixture, which is ignited, leading, in turn, to combustion of the hydrogen fuel. This simulation is restarted from the results obtained in Case II in order to save additional computer time. Detailed experimental results are available from DLR for this case, and consist of schlieren photographs, planar ultra-violet Rayleigh scattering images and Particle Image Displacement Velocimetry (PIV) measurements on the central vertical plane, and side-wall pressure measurements as well as Laser Doppler Velocimetry (LDV) measurements at four vertical lines downstream of the wedge and on the combustor centerline. Since the time-scales of the flow are small, the interactions between the flow, the mixing process and the chemical reaction itself are expected to be important, and the rate at which products (and exothermicity) are formed is likely to be strongly influenced by the rate at which fuel and oxidizer are mixed. The resulting exothermicity is expected to alter the flow, which is conserved under pure mixing, since the dilatation is proportional to the rate-of-change of the density, which in turns mirrors the change in temperature. In particular, the exothermicity is expected to strongly affect the pressure distribution in the combustor, whereas the velocity field is expected to experience only minor changes.

Figure 12 shows experimental and numerical shadow photographs as well as a perspective view from the rear, in terms of velocity, H_2 concentration, temperature and pressure of Case III. With combustion the expansion fans at the upper and lower corners of the wedge vanish, whereas the recompression shocks become weaker as compared to the hydrogen injection case, Case II,

cf. figure 10. With combustion the recirculation region is longer and wider than for Case II, and serves as a flameholder for the hydrogen diffusion flame. Moreover, the peak reverse velocity (in the wake) and the base pressure increase in Case III as compared to Cases I and II. The shear layers, originating at the upper and lower corners of the wedge, are much more pronounced in the combusting case because ignition occurs within the shear layers between the hydrogen rich wake and the freestream air. The flow can roughly be divided into three regions: the induction zone, where the turbulence determines the mixing and the progress of combustion; a transitional zone that is dominated by large-scale coherent flow structures, convective mixing, air entrainment and exothermicity, and a highly turbulent combustion zone, with large-scale coherent structures and mixing. The large-scale structures originate in the shear-layers that roll up, and become increasingly distorted with downstream distance due to vortex breakdown, occupying a large part of the combustor due to the dilatation $\nabla\cdot\tilde{\mathbf{v}}$, resulting mainly from exothermicity. These structures are formed by the interaction of the shocks with the unstable shear-layers. The exothermicity leads to an overall increase in shear-layer thickness, which, in turn, affects the subsequent reflections of the leading shock and the overall combustion chamber pressure. The large-scale structures cause momentum exchange by mixing cold high-momentum air with hot low-momentum hydrogen or product wake flow forcing the transition from subsonic wake flow to supersonic freestream flow, together with exothermicity, within these structures.

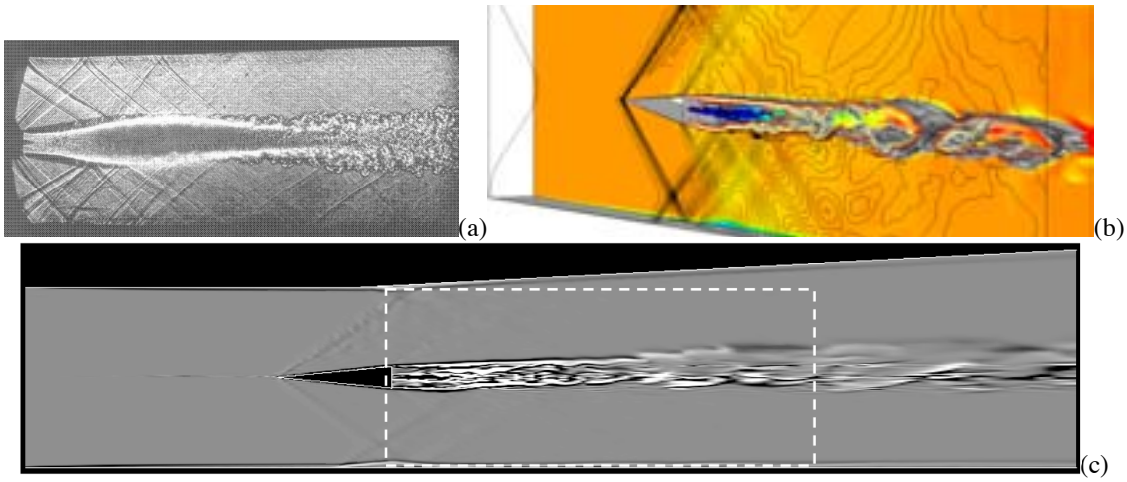

Figure 12. Results from Case III involving supersonic flow in the scramjet combustor with hydrogen injection and combustion. (a) Shadowgraph photographs from the experiments, [49], (b) a perspective view from the rear of the simulated flow and (c) a numerical shadowgraph image from the reacting LES calculations. The size and location of the experimental image (a) is superimposed on (c).

In figure 13 we show additional computational results from the reacting Case III, including numerical estimates of the Rayleigh scattering and the velocity at the centerplane. These results can be compared to the corresponding experimental data of Rayleigh scattering and PIV velocity measurements. The qualitative agreement with the experimental data suggests that the LES are capable of representing the global behavior and the most important physical phenomena of the scramjet test rig, and furthermore that the experimentally observed peculiarities observed in Case III also are present in the LES (see also figure 9). The Rayleigh scattering captures the mixing well due to the abovementioned different Rayleigh-scattering cross sections of fuel, air and combustion products, and clearly shows the entrainment of cold air into the combustion region. The velocity field (with 460 m/s subtracted of the axial or x-component to match with the measured velocity shown in figure 3 in [49]) clearly distinguishes between the high-speed cold freestream

and the low-speed, highly turbulent hot combustion region. Furthermore, the decrease of the velocity after the shocks and the rise of the velocity in the expansion regions is evident. In both figures 13a and 13b the large-scale coherent structures of the transitional and highly turbulent combustion zones are clearly visible.

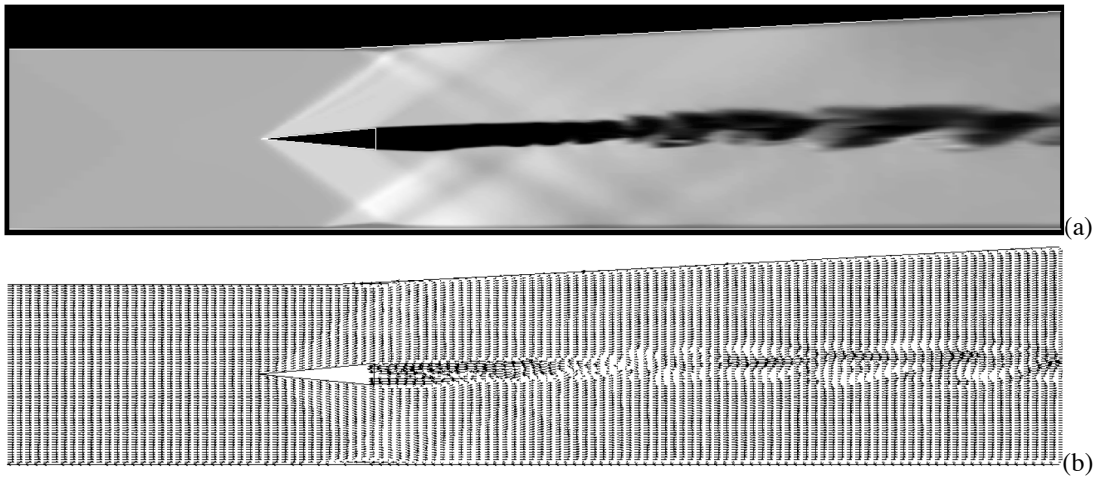

Figure 13. Results from Case III involving supersonic flow in the scramjet combustor with hydrogen injection and combustion. (a) Computationally emulated spontaneous OH-emission intensity and (b) projected velocity in the centerplane (z=0) of the combustor.

In figure 14 we show profiles of the pressure along the lower wall, the time-averaged axial velocity, the axial rms-fluctuations at x/h=13.00, 20.83, 26.16 and 34.50 and the time-averaged temperature at x/h=13.00, 20.83 and 38.83, along with experimental data when available. The time-averaged pressure $\langle \bar{p} \rangle$ at the lower wall (figure 14a) is found to increase considerably in the reacting Case III, as compared to the non-reacting Cases I and II. This is mainly due to exothermicity, causing volumetric expansion, and although the LES calculations does not succeed completely in recovering the values of the wall pressure reported in the experiments the trend is apparent. Reasons for the deviation in $\langle \bar{p} \rangle$ may be due to finite rate chemistry effects or measurement details. Concerning the time-averaged axial velocity $\langle \tilde{v} \rangle_x$ (figure 14b) the LES calculations show reasonable agreement with measurement data in cross-sections with available experimental data. At the first cross-section (x/h=13.00) strong reverse velocity regions are observed on each side of the hydrogen jet(s), and reasonable agreement with the rather sparse experimental velocity profile is obtained. At the second station (x/h=20.83) the predicted velocity defect is narrower than the measured one, which also shows a peculiar and asymmetric shape. In addition, the other LES and 2D RANS calculations, [24-25], show similar profiles as the present one. At the third station (x/h=34.50) good agreement is again obtained, now resulting in an almost flat velocity profile with a constant axial velocity of about 760 m/s. This should be contrasted against the 2D RANS results of Oevermann, [24], predicting a strong overshoot in $\langle \tilde{v} \rangle_x$ at x/h=20.83, which may not only be due to the 2D and steady state assumptions in the RANS model, but may also be due to the RANS laminar flamelet approximation, not taking into account the unsteady coupling between the flow and the chemical reactions. Moreover, the streamwise distribution of $\langle \tilde{v} \rangle_x$ (not shown) along the geometrical centerline of the combustor (y/h=4.16) is also in good agreement with the experimental data, and in particular we find that the velocity drop behind the wedge is surprisingly strong – stronger than for the hydrogen injection case. This observation is in good qualitative and quantitative agreement with experimental data. Concerning the axial rms-fluctua-

tions v_x^{rms} (figure 14c) reasonable agreement is found between the present LES and the experimental data. The amplitude and the width are found within a reasonable accuracy, and the defect that is observed at the centerline is also found in the present simulations. Concerning the time-averaged temperature $\langle \tilde{T} \rangle$ (figure 14d) we find good agreement between the LES and the data at x/h= 13.00 and 38.83, whereas we find that the LES underpredict the peak temperature at around x/h= 20.83, see figure 14c. It is interesting to observe the spatial evolution of the temperature field with downstream distance – the first cross-section is within the induction zone, with mixing controlled combustion, the second is most likely within the transitional zone, with maximum exothermicity, whereas the third is within the highly turbulent combustion zone. Furthermore, we notice that the turbulent wall-boundary layer increases the temperature by almost 200 K due to viscous heating – an effect that influences the thermal load.

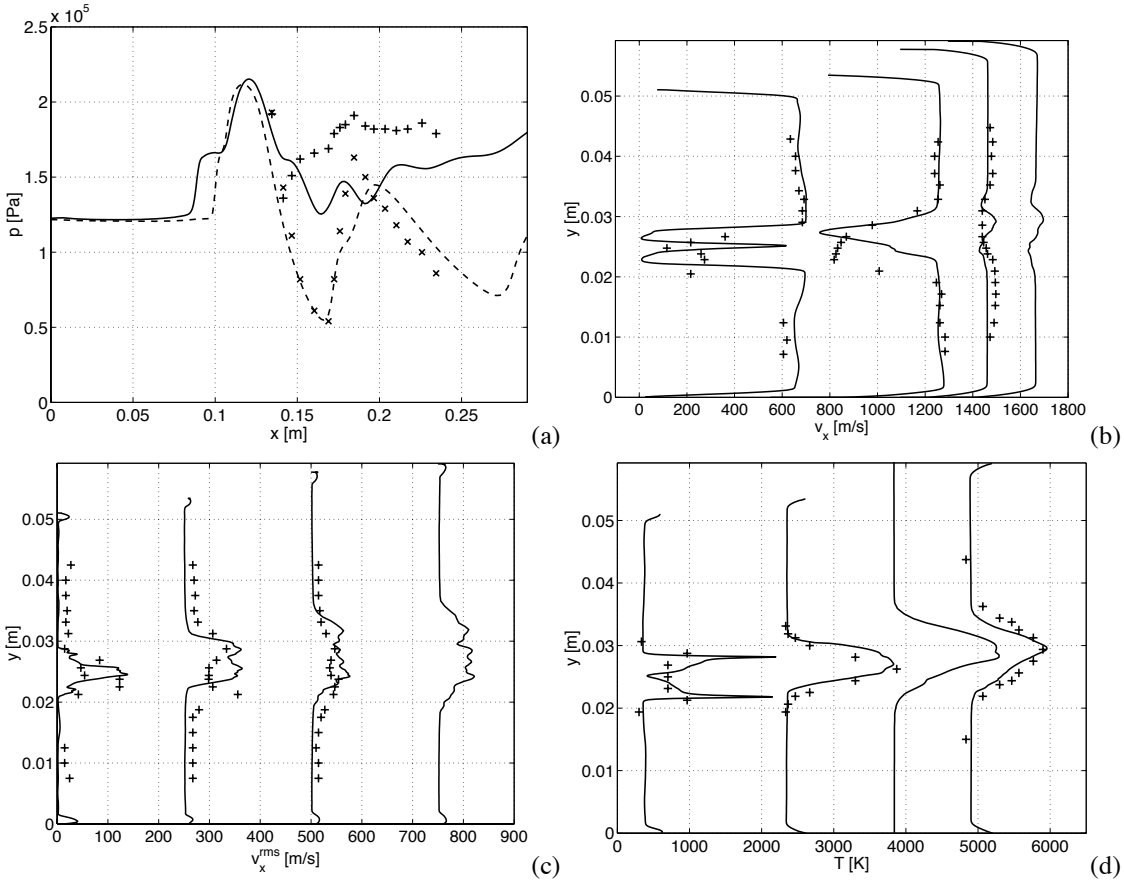

Figure 14. Results from Case III involving supersonic flow in the scramjet combustor with hydrogen injection and combustion. (a) Time-averaged pressure at the lower wall (y=0), (b) time-averaged axial velocity and (c) axial rms-velocity fluctuations at four cross-sections downstream of the wedge at x/h =13.00, 20.83, 26.16 and 34.50 and (d) time-averaged temperature at four cross-sections downstream of the wedge at x/h=13.00, 20.83, 26.16 and 38.8. Legend: Case II is presented by dashed lines and Case III by solid lines, whereas symbols (+ reacting and × non-reacting) are used for the experimental data. Note also that profiles are shifted in the horizontal direction.

7. Concluding Remarks

In the present work LES has been used to investigate supersonic flow, mixing and combustion in a scramjet model under realistic operating conditions. The configuration is similar to the laboratory scramjet developed and experimentally investigated at the Institute for Chemical Propulsion of the German Aerospace Center (DLR). The scramjet model consists of a rectangular, one-sided

divergent channel with a wedge-shaped flameholder at the base of which hydrogen can be injected through a line of holes. In the computational model periodic boundary conditions are used in the spanwise direction (with a span encompassing three holes) to reduce the overall computational cost. The LES model is based on an unstructured finite volume discretization, using total variational diminishing flux reconstruction of the convective fluxes and central differencing for the viscous fluxes. The time integration is fully explicit, using a second order accurate total variational diminishing Runge-Kutta scheme. The LES model itself consists of the filtered continuity, momentum, energy and mixture fraction equations together with algebraic subgrid models for the subgrid turbulent viscosity, heat conductivity and diffusivity of the mixture fraction, as well as for the scalar dissipation rate and the variance of the mixture fraction – the latter quantities being used for the flamelet combustion model. For the reacting scramjet model a mixing controlled turbulent diffusion flame is anchored in the wake of the wedge-like strut, thus acting as a flameholder, whereas combustion is initiated in the shear layers leaving the edges of the wedge. The combustion zone can be divided into an induction zone, from the wedge base to the section where the diffusion flame starts to dominate, a transitional zone, where large-scale coherent structures are developed together with convective mixing, and finally a turbulent (diffusion) flame zone. The pressure in the combustor is almost constant, which is in contradiction to the non-reacting cases also being investigated. Qualitative and quantitative comparisons are systematically made with experimental data for both velocity and temperature for both the non-reacting and reacting cases. These comparisons are supplemented with comparisons of schlieren, shadowgraph, OH-LIF (heat release) and PIV (velocity) fields. In summary, we find that the LES computations are capable of predicting both the non-reacting and reacting flowfields reasonably well – in particular we notice that the LES model identifies and differentiates between peculiarities of the flowfields found in the experiments. The weakest link of this approach is the flamelet model used to model the combustion and turbulence/combustion interactions. An improved flamelet-based LES combustion model have recently been developed, based on a reactive and a non-reactive scalar, instead of a non-reactive scalar only, in order to take into account finite rate chemistry effects, belived to be important in supersonic combustions since the time scales of the flow, mixing and chemistry are closer together than for subsonic combustion. At present, simulations using the new model of the DLR scramjet case are underway, and preliminary results shows improved agreements for all quantities of interest. This continuation of the present will be reported separately in a scientific publication due to its theoretical nature.

Acknowledgement

The authors whishes to acknowledge Dr Torgny Carlsson for valuable discussions concerning the interpretation and the numerical modeling of the light deflection based experimental images.

References

[1] Weber R.J. & MacKay J.S.; 1958, “An Analysis of Ramjet Engines Using Supersonic Combustion”, TN 4386, NACA, September.

[2] Huber P.W., Schexnayder, C.J. & McClinton, C.R.; 1978, “Criteria for Self-Ignition of Supersonic Hydrogen-Air Mixture” NASA TP-1457, August.

[3] Baurle R.A., Fuller R.P., White J.A., Chen T.H., Gruber M.R. & Nejad A.S.; 1998 “An Investigation of Advanced Fuel Injection Schemes for Scramjet Combustion” AIAA-98-0937.

[4] Schetz J.A., Fuller R.P., Wu P.K. & Nejad A.S.; 1996, “Fuel-Vortex Interactions Enhanced Mixing in Super-

sonic Flow," AIAA-96-2661.
[5] King, P.S.; 1989, "Combined Tangential-Normal Injection Into a Supersonic Crossflow" Masters Thesis, Virginia Polytechnic Institute & State University, February.
[6] Sato Y., Sayama M., Ohwaki K., Masuya G., Komuro T., Kudou K., Murakami A., Tani K., Wakamatsu Y., Kanda T., Chinzei N. & Kimura I.; 1992, "Effectiveness of Plasma Torches for Ignition and Flameholding in Scramjet", J. Propulsion and Power, **8**, p 883.
[7] Kato R. & Kimura I.; 1996, "Numerical Simulation of Flame-Stabilization and Combustion Promotion by Plasma Jets in Supersonic Air Streams" Proc. of the 26th Int. Symp. on Comb,, p 2941.
[8] Wagner T.C., O'Brien W.F., Northam G.B. & Eggers J.M.; 1986, "Plasma Torch Ignitor for Scramjets", Presented at the 23rd JANNAF Combustion Meeting, October.
[9] Barbi E., O'Brien W.F., Mahan J.R. & Wagner T.C.; 1989, "Operating Characteristics of a Hydrogen-Argon Plasma Torch for Supersonic Combustion Applications" AIAA J of Propulsion and Power, **5**, p 129.
[10] Kimura I., Aoki H. & Kato M.; 1981, "The Use of a Plasma Jet for Flame Stabilization and Promotion of Combustion in Supersonic Air Flows", Comb. and Flame, **42**, p. 297.
[11] Fujimori T., Murayama M., Sato J., Kobayashi H. & Niioka T.; 1997, "Flame-Holding Behind a Wedge by Incident Shock Waves", IUTAM Symposium on Combustion in Supersonic Flows, p 95.
[12] Davis D.L. & Bowersox R.D.W.; 1997, "Stirred Reactor Analysis of Cavity Flame Holders for Scramjets" AIAA-97-3274.
[13] Yu K., Wilson K.J., Smith R.A. & Schadow K.C.; 1998, "Experimental Investigation on Dual-Purpose Cavity in Supersonic Reacting Flows" AIAA-98-0723.
[14] Baurle R.A. & Gruber M.R.; 1998, "A Study of Recessed Cavity Flowfields for Supersonic Combustion Applications" AIAA-98-0938.
[15] Sands C.J., Milne A.M., Clifford,L.J. & Thomas, G.O.; 1997, "Shock Induced Combustion over a Rectangular Ramp", IUTAM Symposium on Combustion in Supersonic Flows, p 61.
[16] Hartfield R.J., Hollo S.D. & McDaniel J.C.; 1994, "Experimental Investigation of Swept Ramp Injector Using Laser-Induced Iodine Fluorescence" J. Propulsion and Power, **10**, p X.
[17] Donohue J.M., McDaniel J.C. & Haj-Hariri H.; 1994, "Experimental and Numerical Study of Swept Ramp Injection into a Supersonic Flowfield" AIAA J, **32**, p 1860.
[18] Cox S.K., Fuller R.P., Schetz J.A. & Walters R.W.; 1994, "Vortical Interactions Generated by an Injector Array to Enhance Mixing in Supersonic Flow" AIAA-94-0708.
[19] Fuller R.P., Wu P.K., Nejad A.S. & Schetz J.A.; 1996, "Fuel-Vortex Interactions of Enhanced Mixing in Supersonic Flow" AIAA-96-2661.
[20] McCann G.J. & Bowersox D.W.; 1996, "Experimental Investigation of Supersonic Gaseous Injection into a Supersonic Freestream," AIAA J., **34**, p X.
[21] Gruber M.R., Nejad A.S. & Dutton J.C.; 1995, "Circular and Elliptical Transverse Injection into a Supersonic Crossflow – The Role of Large-Scale Structures" AIAA-95-2150.
[22] Achasov O.V., Kondrashov V.V. & Penyazkov O.G.: 1997, "Direct Initiation of Gaseous Detonation by Interacting Supersonic Jets," IUTAM Symposium on Combustion in Supersonic Flows, p 359.
[23] Masuya G., Komuro T., Murakami A., Shinozaki N., Nakumura A., Murayama M. & Ohwaki K.; 1995, "Ignition and Combustion Performance of Scramjet Combustors with Fuel Injection Struts" AIAA J. Propulsion and Power, **11**, p. 301.
[24] Oevermann M.; 2000, "Numerical Investigation of Hydrogen Combustion in a SCRAMJET using Flamelet Modeling", Aerosp. Sci. Tech. **4**, p 463.
[25] Génin F., Chernyavsky B & Menon S.; 2003, "Large Eddy Simulation of Scramjet Combustion using a Subgrid Mixing/Combustion Model", AIAA Paper No. 03-7035.
[26] Hutter K. & Jöhnk K.; 2004, "Continuum Methods of Physical Modeling", Springer Verlag, Heidelberg.
[27] Peters N.; 1993, "Flame Calculations with Reduced Mechanisms – An Outline", In Reduced Kinetic Mechanisms for Application in Combustion Systems, Lecture Notes in Physics (Eds N. Peters and B. Rogg), Springer Verlag, Berlin.
[28] Gutheil E., Balakrishnan G. & Williams F.A.; 1993, "Structure and Extinction of Hydrogen-Air Diffusion Flames", In Reduced Kinetic Mechanisms for Application in Combustion Systems (Eds N. Peters and B. Rogg), Springer Verlag, Berlin.
[29] Rogers R.C. & Chinitz W.; 1982, "On the use of Hydrogen-Air Combustion Model in the Calculation of Turbulent Reacting Flows", AIAA Paper No 82-0112.
[30] Trevino C. & Mauss F.; 1993, "Structure and Extinction of Non-Diluted Hydrogen-Air Flames", In Reduced Kinetic Mechanisms for Application in Combustion Systems (Eds N. Peters and B. Rogg), Springer Verlag, Berlin.
[31] Balakrishnan G., Trevinio C. & Mauss F.; 1992, "The Asymptotic Structure of Hydrogen-Air Diffusion Flames", Comb. Flame., **91**, p 246,
[32] Jones W.P.; 1993, "Turbulence Modeling and Numerical Solution Methods for Variable Density and Combusting Flows", p 309, in Turbulent Reacting Flows (eds. Libby P.A. & Williams F.A.), Academic Press.

[33] Pope S.B.; 2000, “Turbulent Flows”, Cambridge University Press.
[34] Launder B.E., Reece G.J & Rodi W.; 1975, “Progress in the Development of a Reynolds Stress Turbulence Closure”, J. Fluid Mech., **68**, p 537.
[35] Sagaut P.; 2001, “Large Eddy Simulation for Incompressible Flows”, Springer Verlag, Heidelberg.
[36] Bensow R., Persson T. & Fureby C., 2005, “Reformulation of the Incompressible LES Equations with Implications on Subgrid Modeling”, Submitted to Phys. Fluids.
[37] Menon S.; 2001, “Subgrid Combustion Modeling for Large-Eddy Simulations of Single and Two-Phase Flows”, Advances in LES of Complex Flows, Eds. Friedrich R. & Rodi W., p 329, Kluwer, The Netherlands.
[38] Grinstein F.F. & Kailasanath K.K; 1994, “Three Dimensional Numerical Simulations of Unsteady Reactive Square Jets”, Comb. & Flame, **100**, p 2.
[39] Poinsot T. & Veynante D.; 2001, “Theoretical and Numerical Combustion”, Edwards.
[40] Pope S.B.; 1985, “PDF Methods for Turbulent reactive Flows”, Prog. Energ. Comb. Sci., **11**, p 119.
[41] Sankaran V. & Menon S.; 2003, “Sub-grid Combustion Modeling for the Next Generation National Combustor Code”, CCL Report 2003-009, Georgia Institute of Technology, Atlanta, GA, USA.
[42] Williams F.A.; 1985, “Combustion Theory”, Benjamin-Cummings, Menlo Park.
[43] Peters N.; 1984, “Laminar Diffusion Flamelet Models in Non-Premixed Turbulent Combustion”, Prog. Energ. Comb. Sci., **10**, p 319.
[44] Maas U. & Warnatz J.; 1988, “Ignition Processes in Hydrogen-Oxygen Mixtures”, Comb. Flame., **74**, p 53.
[45] Hirsch C.; 1999, “Numerical Computation of Internal and External Flows”, J. Wiley & Sones.
[46] Gurtin M.. E.; 1981, “An Introduction to Continuum Mechanics”, Academic Press, Orlando.
[47] van-Leer B.; 1974, “Towards the Ultimate Conservation Difference Scheme I. The Quest of Monotonicity“, J. Comp. Phys., **14**, p 361.
[48] Gottlieb S. & Shu C.-W.; 1998, “Total Variational Diminishing Runge-Kutta Schemes”, Mathematics of Computation, **67**, p 73.
[49] Oschwald M., Guerra R. & Waidmann W.; 1993, “Investigation of the Flowfield of a Scramjet Combustor with Parallel H_2-Injection through a Strut by Particle Image Displacement Velocimetry”, Int. Symp. On Special topics in Chem. Prop., p 498, May 10-14, Schweveningen, NL.
[50] Waidmann W., Alff F., Brummund U., Böhm M., Clauss W. & Oschwald M.; 1994, “Experimental Investigation of the Combustion Process in a Supersonic Combustion Ramjet (SCRAMJET)”, DGLR Jahreszeitung, Erlangen.
[51] Waidmann W., Brummund U. & Nuding J.; 1995, “Experimental Investigation of Supersonic Ramjet Combustion (SCRAMJET)”, 8th Int. Symp. on Transp. Phenom. In Comb., p 1473.
[52] Waidmann W., Alff F., Brummund U., Böhm M., Clauss W. & Oschwald M.; 1995, “Supersonic - Combustion of Hydrogen/Air in a Scramjet Combustion Chamber”, Space Tech. **15**, p 421.
[53] Fureby C., Alin N., Wikström N., Menon S., Persson L., & Svanstedt N.; 2004, “On Large Eddy Simulations of High Re-number Wall Bounded Flows”, AIAA.J. **42**, p 457.
[54] Eckbreth A. C.; 1996, “Laser Diagnostics for Combustion Temperature and Species”, Gordon & Breach Publ.
[55] Hall J.L., Dimotakis P.E. & Rosemann H.; 1991, “Some Measurements of Molecular Mixing in Compressible Turbulent Shear Layers”, AIAA 91-1719.